TECHNISCHE UNIVERSITÄT WIEN

DIPLOMA THESIS

Single-Molecule Characterization of mStayGold Variants for Fluorescence Microscopy

Author:
Matthias Florentin Paul, BSc

Supervisor:
Univ. Prof. Dipl.-Ing. Dr. techn. Gerhard Schütz
Dipl.-Ing. Dr. techn. Mario Brameshuber

A thesis submitted in fulfillment of the requirements for the degree of Diplom-Ingenieur

in

Biomedical Engineering

at the

Institute of Applied Physics
Biophysics Group

January 31, 2025

Declaration of Authorship

I, Matthias Florentin Paul, BSc, declare that this thesis titled, "Single-Molecule Characterization of mStayGold Variants for Fluorescence Microscopy" and the work presented in it are my own. I confirm that:

- This was done wholly in candidature for a research degree at this University.
- Where any part of this thesis has previously been submitted for a degree or any other qualification at this University or any other institution, this has been clearly stated.
- Where I have consulted the published work of others, this is always clearly attributed.
- Where I have quoted from the work of others, the source is always given. With the exception of such quotations, this thesis is entirely my own work.
- I have acknowledged all main sources of help.
- Where the thesis is based on work done by myself jointly with others, I have made clear exactly what was done by others and what I have contributed myself.

Signed: 

Date: 31.01.25

Abstract

Fluorescent proteins (FPs) are essential in modern biophysical and biochemical research, particularly in fluorescence microscopy of living cells. In combination with single-molecule microscopy techniques, they enable visualization of specific organelles or receptors beyond the diffraction limit, allowing for detailed insight into biological processes at the nanoscale. This work explores recent advancements in the development of more photostable and bright FPs, focusing on their potential to enhance the tracking ability and expand the range of applications where traditional monomeric enhanced green flourescent protein (EGFP) has reached its limitations.
This study investigates the three newly developed monomeric StayGold variants (mStayGold-E138D, mBaoJin and mStayGold) and compares their performance to conventional mEGFP. The mStayGold variants are reported to be brighter and much more photostable than all currently available alternatives. While previous studies on the new mStayGold variants tested these properties in various bulk experiments in live-cell applications, this work will provide a detailed characterization of their brightness and photostability at the single-molecule level. To achieve this, a cell-mimicking platform was established using supported lipid bilayers containing DGS-NTA-Ni lipids for the attachment of the Histidine-tagged FPs. To ensure accurate single-molecule localization and tracking, two different software approaches were applied: *ThunderSTORM*, an ImageJ localization plugin coupled with a custom MATLAB script for tracking and *DaoSTORM*, a Python plugin in combination with *Trackpy* and *std-python*. The resulting tracking data underwent extensive Python-based analysis, generating statistics on brightness, on-times (duration a FP is active), off-times (duration a FP is inactive), total number of localizations and total number of gaps (blinking events).
The results on immobile FPs reveal that, compared to mEGFP, mStayGold demonstrates a marked improvement in single-molecule brightness (+25%), on-time (+55%) and total number of localizations (+145%) per recording while reducing the off-times (-25%), leading to a substantial overall enhancement in photostability and fluorescent output. The mBaoJin variant displayed similar properties as mStayGold, with marginal reductions across all metrics. However, the mStayGold-E138D variant did not show significant improvements in brightness or on-times, a small decrease in off-times and an marginal total increase in localizations. All results were validated for both mobile and immobile proteins, under varying excitation doses (150-1200 W/cm² and 80 to 1 ms illumination times) and in bulk bleaching experiments to create a comprehensive assessment of the FPs single-molecule performance.
Additionally, we explored approaches to further improve the photostability without the need for additional hardware by introducing stroboscopic illumination. Splitting the continuous illumination into two microsecond bursts resulted in increased single-molecule half-times compared to mEGFP of up to 30% for mBaoJin and up to 76% for mStayGold under optimized settings.
In total, the findings support that mBaoJin and mStayGold are strong candidates for single-molecule applications, offering substantially improved single-molecule brightness and photostability across various experimental settings compared to mEGFP.

Acknowledgements

First let me say: Great thanks to all members of the biophysics group! You took me in so kindly and have all always supported me throughout my studies. Some people were particularly invested over the last few years, leading to this day, making this thesis possible. Lukas V. and Benedikt, who were the first to support me during my bachelor thesis and gave me a glance of what can be done in biophysics. Then Caro and Mario, who supported me during my project thesis, making it a great and also enjoyable learning experience. Finally, this diploma thesis took my scientific work to the next level thanks to the invaluable support of Mario, who continuously amazed me with new layers of depth in our research and supported me with his kind supervision. Lastly, also Barbora, who always helped me out during my research when I was in trouble, especially but not exclusively in providing the proteins used. It was a pleasure working with you all!

All of this would not be possible without Gerhard, the person who brought me into this field many years ago through his great lectures and was a constant advisor throughout all of these studies. His enthusiasm and offbeat thinking sparked my interest in joining the wonderful world of biophysics and I enjoyed every minute of it. Thank you!

Most importantly, all thanks of the world go to my parents, these wonderful, kind and loving people who always supported me in all imaginable ways and thereby made all of it possible.

To all the other amazing people in my life who made this happen: thank you!

Contents

Declaration of Authorship i

Abstract ii

Acknowledgements iii

1 Introduction 1
- 1.1 Fluorescence microscopy . . . 1
- 1.2 Labeling strategies . . . 4
  - 1.2.1 Fluorescent proteins . . . 5
  - 1.2.2 StayGold . . . 6
- 1.3 Model system for characterization . . . 10
- 1.4 Aim of the work . . . 12

2 Methods 13
- 2.1 Bilayer preparation . . . 13
  - 2.1.1 Mobile bilayer . . . 13
  - 2.1.2 Immobile bilayer . . . 14
- 2.2 Proteins . . . 14
- 2.3 Experimental microscopy setup . . . 14
- 2.4 Data processing . . . 17
  - 2.4.1 DaoSTORM + Trackpy . . . 17
  - 2.4.2 ThunderSTORM + MATLAB . . . 18
  - 2.4.3 Further calculations . . . 19

3 Results and Discussion 21
- 3.1 Bulk photobleaching . . . 21
- 3.2 Single-molecule measurement . . . 24
  - 3.2.1 Single-molecule Blinking . . . 26
  - 3.2.2 Single-molecule Brightness . . . 32
- 3.3 Bulk vs. single-molecules . . . 35
- 3.4 Mobile vs. immobile proteins . . . 36
- 3.5 Varying excitation doses . . . 37
- 3.6 Stroboscopic illumination . . . 40

4 Conclusion 44

A Additional information 50

Chapter 1

Introduction

1.1 Fluorescence microscopy

To truly understand how living organisms function, it is essential to observe the biophysical mechanisms that drive these processes, often requiring highly sophisticated imaging techniques. This is particularly challenging when examining complex systems such as the immune response, involving a wide variety of players, each with specific and crucial roles that are still far from fully understood. For instance, visualizing single-cell surface receptors, which are crucial in immune signaling, is particularly challenging due to their constant movement and interactions with other proteins. Additionally, all processes concerning receptors typically occur below the diffraction limit of visible light, making them impossible to visualize with standard light microscopy techniques. To specifically visualize single receptors, one effective approach is to use fluorescence microscopy. This approach employs fluorophores that specifically target the molecules of interest, like organelles, receptors, or other molecules, and use their photon emission for recording, making it possible to track and visualize them very precisely. The fundamental mechanism behind fluorescence microscopy lies in the process of fluorescence emission. Emission occurs when a fluorophore is excited into a higher atomic singlet state S_1 and subsequently relaxes into the ground state S_0, emitting a photon in the process (Figure 1.1). The energy input for excitation to the S_1 state is provided from the excitation light source at a specific wavelength λ_1 while the photon emission occurs in the form of emission of a photon with a specific wavelength λ_2 showing the characteristic Stokes shift (Equation 1.1, h...Planck constant, c...speed of light), resulting from relaxation of vibrational states in the excited S1 state or loss of energy through reaction with the solvent. The emission signal is then typically brought to the user by projection on a camera chip.

$$\Delta E_{Stokes} = E_2 - E_1 = hc(\frac{1}{\lambda_2} - \frac{1}{\lambda_1}) \tag{1.1}$$

However, achieving high specificity and labeling density is crucial to ensure that the fluorescent markers label exclusively to the receptor of interest and do not visualize unintended structures. When working with cells, an additional challenge arises due to the density and distribution of receptors across the three-dimensional surface. Direct illumination through the whole cell leads to significant background signal and noise, obscuring the fine details of molecular interactions. As a special illumination approach for minimizing background signal, this work employs total internal reflection microscopy (TIRFM) [1]. In this technique, the incoming angle of excitation laser light is adjusted to match the critical angle Θ_c of total reflection (Equation 1.3), resulting directly from Snell's law (Equation 1.2) when the object medium angle Θ_2 is reaching an angle of 90 degrees (Figure 1.2).

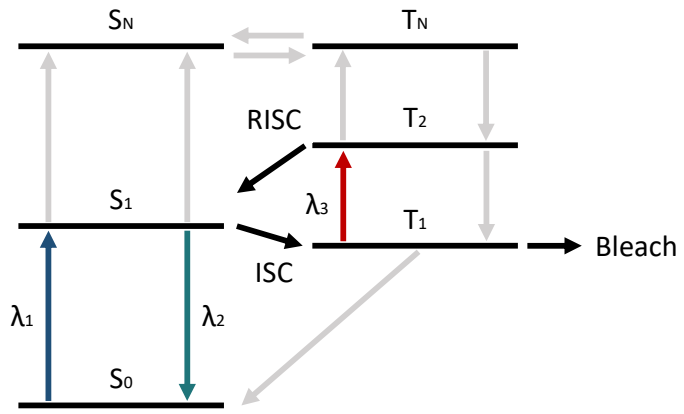

FIGURE 1.1: The Jablonksi energy level diagram of a fluorescent molecule is showing the singlet states Sx and the triplet states Tx. The excitation wavelength λ1, the emission wavelength λ2 and the near-infrared excitation wavelength λ3 are represented in color. The intersystem crossing (ISC), the reverse intersystem crossing (RISC), as well as the primary photobleaching path are shown in black, while the other possible transition processes are shown in gray.

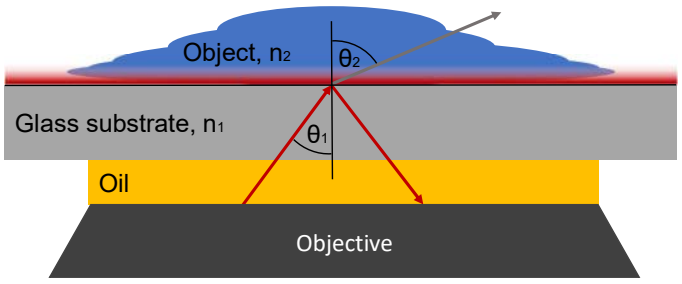

FIGURE 1.2: TIRF microscopy concept with n_1...approaching medium refractive index, n_2...object medium refractive index, θ_1...approaching medium angle, θ_2...object medium angle and θ_c...critical angle.

$$n_1 * sin(\theta_1) = n_2 * sin(\theta_2) \tag{1.2}$$

$$sin(\theta_c) = \frac{n_2}{n_1} \tag{1.3}$$

While, at a macroscopic scale, there would be no light transmitted on the sample after the glass sheet, an evanescent wave is generated at the interface between the glass and the sample in TIRFM. By considering a light beam as a combination of parallel transverse magnetic (TM) and perpendicular transverse electric (TE) polarized electric field vectors, the electromagnetic field within the object can be derived directly from Maxwell's equations [2]. The field oscillates with the wavelength of the approaching light λ and its intensity I(z) decreases exponentially in the direction of the optical path z depending on the initial intensity at the glass slide surface $I_{12}(0)$ (Equation 1.4). The penetration depth d_{12} of the field is defined by the refractive indices n_1 as well as n_2 and the wavelength λ of the incoming beam (Equation 1.5).

$$I(z) = I_{12}(0) * e^{-\frac{z}{d_{12}}} \tag{1.4}$$

$$d_{12} = \frac{\lambda}{4\pi\sqrt{n_2^2 sin^2(\theta) - n_1^2}} \tag{1.5}$$

Typical numbers (cover glass n_1=1.523, cell cytosol n_2=1.38 and laser wavelength λ=488 nm) result in a penetration depth of d_{12} of approximately 100 nanometers, corresponding to a 1/e decay of the initial intensity at that depth. This limited illuminated depth is sufficient to exclusively excite fluorophore-labeled receptors of interest that are located close to the bottom of a cell, illuminating all processes of interest. As a result, TIRF microscopy drastically reduces the background noise of the image, as only those fluorophores contribute to the signal.

Single-molecule microscopy

In a diffraction-limited system, the resolution can be defined by the Abbe diffraction limit (Equation 1.6).According to this principle, imaging a structure with periodicity d requires at least the first diffractive order to pass through the objective lens aperture, which depends on the wavelength λ and the numerical aperture NA. Inserting the wavelength of a blue 488 nm laser and a typical NA for an oil immersion objective of 1.45 results in a resolution of 168 nm. In respect to GFPs with diameters of several nanometers or entire T-cells in the range of micrometers, it becomes clear that this resolution is not sufficient for resolving structures in cells using fluorescence microscopy.

$$d = \frac{\lambda}{2 \cdot \mathrm{NA}} \tag{1.6}$$

However, by combining fluorescent labeling strategies and advanced microscopy techni-ques, it is possible to visualize structures with details smaller than that limit, enabling the visualization of individual molecules in living cells. Following the development of the fundamental principle of single-molecule microscopy, stimulated emission depletion (STED) by Hell et al. [3], which uses selective deactivation of fluorophores to overcome the diffraction resolution, multiple new approaches have emerged. These include single-molecule localization microscopy (SMLM), which reconstructs sub-diffraction-limited images from a sequence of diffraction-limited images in the wide-field. Techniques such as stochastic optical reconstruction microscopy (STORM) [4] or photoactivated localization microscopy (PALM) [5] are examples of SMLM. All single-molecule microscopy approaches utilize fluorescent labeling of single emitters combined with sophisticated algorithms to localize individual fluorophores with strongly improved precision by fitting single point spread functions (PSF) instead of simultaneous measurement of multiple diffraction-limited fluorophores. Methods for localizing single PSF include separating the blinking events in time (STORM) or switching fluorophores on and off in a controlled manner (PALM). The subsequent reconstruction of images leads to significantly improved resolution, allowing for improved observation of molecular dynamics, interactions and behaviors in living cells.
There are also other approaches available that use vizualize single emitters by introducing decreased labeling densities or photobleaching of specific regions, like thinning out clusters while conserving the stoichiometry of labeling (TOCCSL) [6]. This approach, for example, allows not only for the observation of single-labeled surface

receptors of T-cell antigen recognition but also, by measuring the signal intensity alongside specific labeling techniques, allows for the identification of monomericity or dimericity of those receptors in living cells [7].

1.2 Labeling strategies

Selecting the best labeling strategies for an experiment is essential and must be customized to the specific application [8]. The type of label used dictates the visualization method for the biomolecule of interest and offers different benefits and drawbacks. Thereby, it is crucial that the biological functionality of the molecules remains unaffected by the labeling process. Generally, two types of fluorophores are available, fluorescent proteins or fluorescent dyes. Fluorescent dyes such as ATTO, CyX or Alexa-Fluor groups are in general brighter and more photostable. Their small size makes them highly attractive for fluorescence microscopy applications, especially when minimal-invasive conjugation to the biomolecules of interest is desired. However, a major limitation is the need for labeling via functional groups like antibodies or antibody-fragments (Fab) to target specific regions of interest, which can make achieving precise labeling difficult (Figure 1.3a, b). In contrast, fluorescent proteins like the green fluorescent protein (GFP) or proteins from GFP sub-families can be genetically encoded and expressed directly within living cells, allowing for direct visualization in the organelles of interest with high specificity (Figure 1.3c). This ability makes fluorescent proteins particularly advantageous for non-invasive, real-time imaging of cellular processes and dynamic events in live cells. Nevertheless, genetically encoding fluorescent proteins in cells can lead to strong background signals due to their potential high abundance in the cytosol and inner membranes.

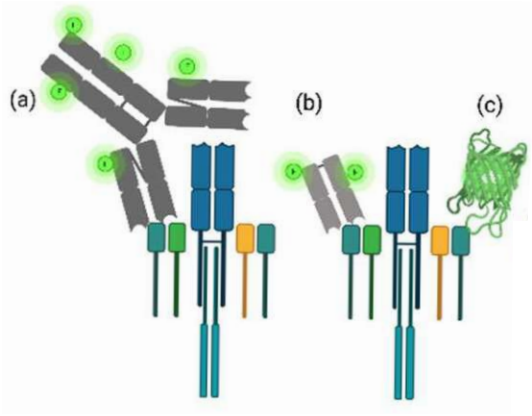

FIGURE 1.3: Examples for labeling concepts on a TRC/CD3 complex from [8]. The concepts include: (a) primary NHS-labeled antibody holding multiple fluorescent dyes; (b) Fabs with randomly labeled NHS-functionalyzed organic dyes; or (c) genetically fused fluorescent proteins.

For precise analysis, it is ideal for each molecule of interest to carry exactly one fluorophore, achieving a 1:1 labeling stoichiometry of molecule to fluorophore. This can theoretically be accomplished through the genetic attachment of FPs, but factors such as maturation efficiency and incorrect protein folding can affect this process. Also, fluorescent dyes in combination with nanobodies can theoretically achieve near-perfect stoichiometry due to their strong specificity. However, antibodies can cause cross-linking due to their divalent nature and Fabs can carry more than two

organic dyes linked via NHS labeling [8]. This behavior directly influences the resulting brightness distributions and thus affects experiments focusing on colocalization or brightness analysis. Additionally, quenching can happen for many dyes when they are in close proximity on a single label.
Ultimately, the choice of labeling strategy must be carefully considered based on the experiment's specific requirements. In this work, we focus on characterization and improvement of fluorescent proteins coming from the family of green fluorescent proteins (GFPs).

1.2.1 Fluorescent proteins

Since the first extraction of GFP from the jellyfish Aequorea victoria in 1962 [9] and the first cloning for scientific use in cell biology in 1992 [10], GFP has become one of the most invaluable tools in molecular and cellular biology. Subsequently, more and more different types of fluorescent proteins were discovered also from different organisms, like mCherry, a protein emitting wavelengths in the red spectrum that was derived from dsRed originating from sea anemones. Today, hundreds of different variants for specific purposes are available and the research is still ongoing. The original GFP molecule consists of its typical beta-barrel structure that holds and protects the light-emitting chromophore inside. Further advancements of new forms of GFP are made by mutation and selection to achieve specific biological features. Every type of GFP has a specific excitation and emission spectrum that defines the color range. Organic dyes emit photons following irradiation, following the same model as fluorescent proteins and are available in a range of colors, allowing high spectral diversity in multi-color imaging. However, when choosing a fluorophore for an experiment, there are still many factors to consider, such as potential influences on cellular functionality, potential blocking of binding sites, or other unintended effects. For effective tracking and visualization, the primary challenge remains the relatively reduced brightness and limited photostability of fluorescent proteins compared to dyes. Addressing these limitations would enhance their applicability in detailed, long-term studies of dynamic processes within living cells.

Photobleaching

The primary limitation in fluorescence microscopy using fluorescent proteins is photobleaching. Each type of fluorescent protein possesses a characteristic photostability, which is determined by the protein molecular structure and can be influenced by factors such as the excitation intensity or the excitation method from the microscopic approach. Photobleaching arises because the excited fluorophores tend to react with surrounding reactive molecules in the environment, particularly molecular oxygen. The resulting reactive oxygen species (ROS) can further react with either the fluorophores themselves or with the surrounding biological structures, leading to phototoxicity. Although multiple energy states may be involved in photobleaching, each with their respective transition probabilities and lifetimes, the primary contributor is the first triplet state T1, which has a relatively long lifetime of approximately one microsecond while not contributing fluorescent output [11]. The excitation to bleaching states can either occur when fluorophores absorb excess energy beyond S1 or through intersystem crossing (ISC). In ISC, the excited fluorophore transitions directly from the excited singlet state to the bleaching triplet state (Figure 1.1). Literature [11] suggests that further irradiation of a molecule in the T1 state with a red-shifted laser would lead to reverse intersystem crossing (RISC), restoring the S1,

reducing photobleaching and enabling photon emission.

To reduce photobleaching, the initial approach would be to minimize both excitation energy and illumination time, limiting excess excitation of the fluorophores while ensuring the fluorescence output meets the application requirements. Another common strategy involves reducing the oxygen of the fluorophore environment, as the oxygen promotes the photobleaching and phototoxicity. However, the reduction of oxygen may affect the health or behavior of the cells in live-cell microscopy. Also, in the work of Cordes et al. [12] they found that the two anti-fade substances for oxygen scavenging they used did not result in significantly reduced photobleaching of antibody-labeled GFP, while they were effective for organic dyes like Alexa488, ATTO647 or Cy3B. Reducing photobleaching in fluorescent proteins from the excitation side, literature suggests several innovative techniques that avoid or minimize hardware modifications or changes in the experimental preparation steps. Donnert et al. [13] demonstrated that photobleaching can be strongly reduced when the relaxation time between two absorption events of a fluorophore is longer than the molecular dark-state duration of the triplet state T1 of typically one microsecond, ensuring relaxation to the ground state S0. Short excitation pulses separated by intervals greater than one microsecond, while keeping the total time of excitation constant, showed strongly decreased photobleaching in GFP. De et al. [14] varied the excitation pulse length and found that nanosecond pulses (1-100 nanoseconds) in combination with relaxation times of greater than one microsecond yield the best fluorescent output in their experiments. Similarly, Boudreau et al. [15] adapted the effect to confocal laser scanning microscopy (CLSM), finding that increased line scanning speeds that lead to shorter pixel dwell times (12 to 1 microsecond) also resulted in decreased photobleaching of EGFP. Another innovative approach to decrease photobleaching with limited hardware addition to the microscopy setup is near-infrared (NIR) co-illumination. In this technique, a NIR laser is added to the imaging pathway to excite fluorophores in the highly reactive first triplet state towards a higher triplet state, promoting a transition back to the singlet state (RISC), where it can return to the ground state without photobleaching while contributing to the fluorescent output by emitting a photon [16]. The optimum wavelength matching the transition energy of this process was found to be at 900 nanometers for EGFP by determining a maximum in the absorption spectrum [17]. Nevertheless, all results from both approaches were derived from bulk fluorescence samples without examining the true single-molecule signals of the fluorescent proteins.
All approaches in fluorescent microscopy are dependent on the photostability and brightness properties of the fluorophores used and optimizing these properties would be highly beneficial. Many different improved variants of GFP are available today and the advancements are still ongoing.

1.2.2 StayGold

One groundbreaking contribution to the research of fluorescent proteins of the last years, which this work will explore in depth, is StayGold. This fluorescent protein is reported to show exceptional brightness and photostability compared to all other available fluorescent proteins. StayGold, first developed by Hirano et al. [18], is a single-point-mutated fluorescent protein derived from the original CU17S protein that was extracted from the jellyfish *Cytaeis uchidae* (Figure 1.4). Each of the resulting dimer subunits is composed of an 11-stranded beta-barrel, almost identical to

the GFP of *A. victoria*. The fluorophore is located at the center of the barrel and notably, through mutations, it features the presence of a chloride ion right beside the fluorophore. Still, further investigation is needed to fully understand the role of the chlorine ion in the brightness of StayGold [19]. Hirano et al. expressed the 40 kDa protein in living HeLa cells and excited them with 5.6 W/cm² continuous wide-field illumination (Figure 1.5a). The resulting normalized photobleaching curves compared to other currently available fluorescent proteins showed that StayGold is over an order of magnitude more photostable while maintaining strong cellular brightness.

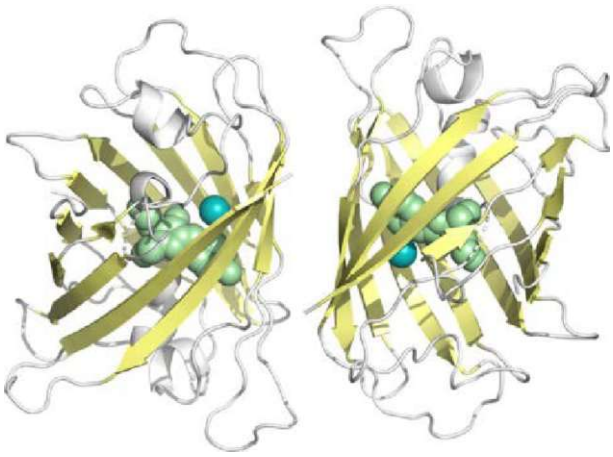

FIGURE 1.4: The molecular structure of the StayGold dimer showing the two subunits, including the beta barrel (gold), the fluorophore (green), and the chloride ion (blue) [19].

However, this initially published version of the protein was expressed only as a dimer, which limits its suitability for single-molecule applications. The dimerization poses challenges for certain applications, such as protein tagging, the study of protein-protein interactions, such as in Förster resonance energy transfer (FRET) applications, or simply by their size and binding characteristics [20]. The first monomeric StayGold variant, named mStayGold, was introduced by Ando et al. [21], the same group that developed the original dimeric StayGold. They gradually introduced mutations into the dimeric interface to disrupt the dimerization while maintaining or even enhancing its strong photostability and brightness. During the process of mutation and screening using assays such as OSER (assay for assessment of monomericity and dispersibility) and FLUOPPI (fluorescent protein-protein interaction assay), they identified multiple variants suited for various applications. They finally came up with a variant (QC2-6 FIQ) that was exhibiting exceptional brightness and photostability (Table 1.1) while showing strong scores for monomericity in both OSER (92%) and FLuoppi (100%), an fluorescent-based technology detecting protein-protein interactions.
Shortly afterward, Ivorra-Molla et al. [19] developed another monomeric StayGold approach. They also mutated the dimerization interface, generating several variants that are monomeric. Among these, the version named mStayGold-E138D demonstrated the highest monomericity (99%, size-exclusion chromatography) and was named for its characteristic mutation position at GLU138 (Figure 1.5c). The monomerization arises from several effects. One is the shortening of the negatively charged side chain due to the GLU substitution, causing repulsion between the monomers. One other factor is that the mutations also disrupt stabilizing hydrogen bonding at the dimer interface. The mSG-E138D and mStayGold variants reportedly have

nearly identical excitation and emission maxima, alongside similar quantum yields (Table 1.1).
Following these, Zhang et al. [22] introduced another variant called mBaoJin, which is reported to exhibit exceptional photostability and chemical stability. After eight rounds of direct evolution by selecting the brightest colonies, they identified a bright monomeric variant, which they further optimized by incorporating the NC termini from the mNeonGreen protein to ensure stability in mammalian cells. They confirmed 99% monomericity at high protein concentrations using fast protein liquid chromatography (FPLC). X-ray structure analysis revealed two internal mutations to the beta barrel and six external mutations. Notably, while the chromophore of mBaoJin was more planar at acidic pH values, a chloride pocket near the chromophore, similar to StayGold, was found in all settings, leaving the molecular brightness of mBaoJin practically unaffected by pH changes. The entire emission spectra for mStayGold, mSG-E138D, mBaoJin, and mEGFP are also depicted in Figure 3.16. The full genetic codes are shown in Appendix A.

Protein	Ex/Em [nm]	QY	EC	Ref.	[23] Cellular brightness	[23] Photostability $T_{1/2}$
mEGFP	488/507	0.6	56	[24]	ND	ND
mStayGold	499/510	0.83	164	[21]	1.47±0.45	5,226±410
mSG-E138D	497/504	0.87	145	[19]	0.37±0.19	4,975±267
mBaoJin	500/508	0.93	128	[22]	1.01±0.26	1,104±59

TABLE 1.1: Characteristics of mEGFP and the mStayGold variants, including the excitation and emission wavelength, the quantum yield (QY), and the molar extinction coefficient (EC). On the right half, a direct comparison from Shimonozo et al. [23] of the cellular brightness and photostability half-life in an organized smooth ER (OSER) assay after protein fusion to the C-terminus of CytERM for ER-membrane targeting in fixed HeLa cells, is shown. (ND = not defined)

Characteristics of new mStayGold variants

The results from the original research papers of StayGold and each mStayGold variant demonstrate the photostability and brightness enhancements of these proteins using a range of microscopy techniques, including wide-field illumination, spinning disc confocal microscopy (SDCM) and structured illumination microscopy (SIM). In each study, the expression of the fluorescent proteins in cells was achieved through different approaches, including gene re-synthesizing with mammalian-preferred codons for direct expression in HeLa cells [18], fusion with tropomyosin-2 for expression in fixed human RPE-1 cells [19], fusion to H2B in HeLa cells [21] or implementing the P2A self-cleavage peptide method in HEK cells [22] (Figure 1.5a-c). The resulting photobleaching curves for dimeric StayGold under continuous illumination (Figure 1.5a) demonstrate a remarkable 20-fold increase in half-time compared to mEGFP. Similarly, mStayGold exhibits significantly prolonged half-times under high-energy (1 kW/cm²) laser-based illumination (Figure 1.5b), while the half-time increase in respect to mEGFP reduces to approximately 5-fold. Further, it was shown that mStayGold-E138D has very similar photostability performance as mStayGold under continuous low-energy illumination (7.4 W/cm²) (Figure 1.5c). Figure 1.5d highlights that mStayGold is 1.9 to 2.3-fold more photostable than mBaoJin during

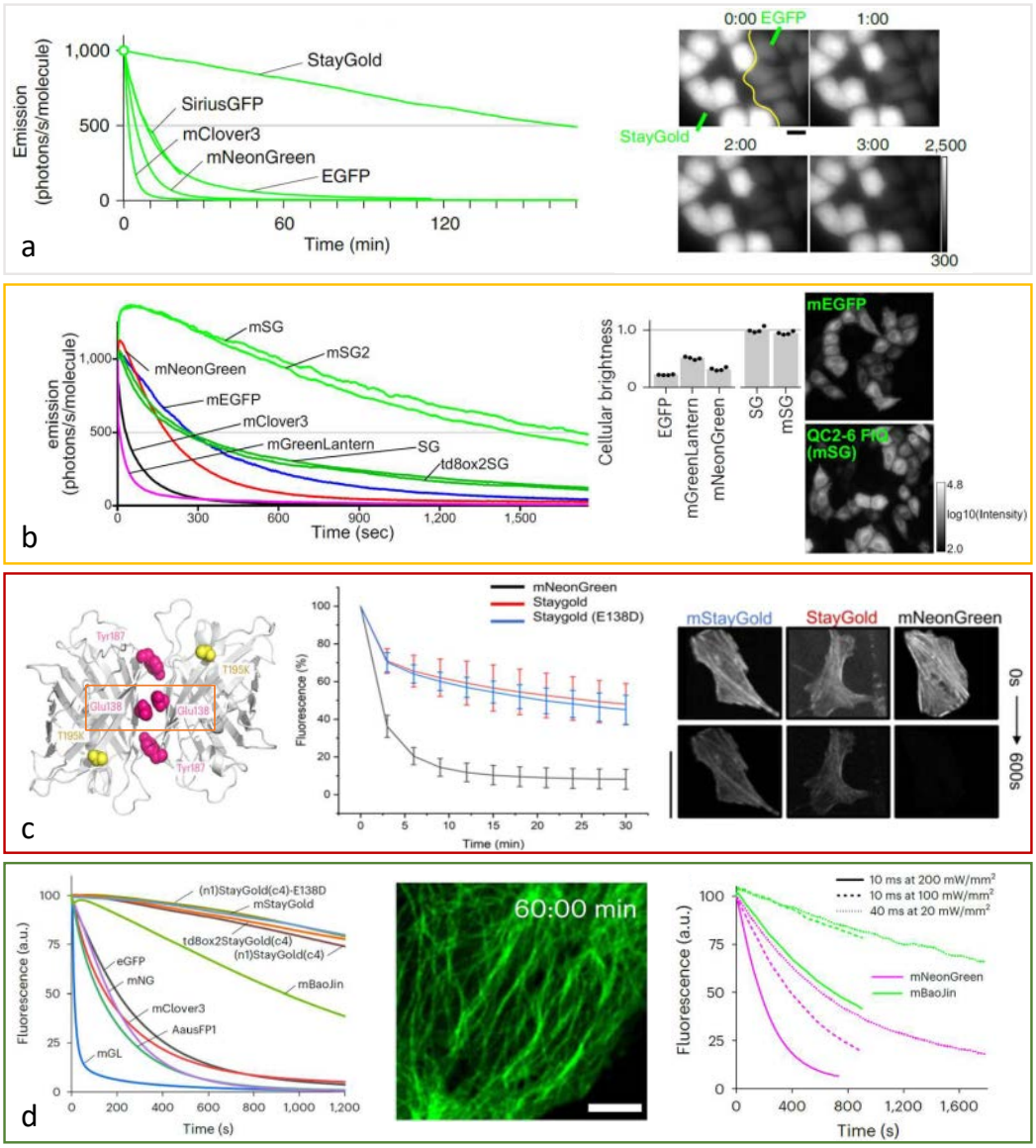

FIGURE 1.5: Results from literature on StayGold: **a**, the StayGold characterization [18] showing the normalized photobleaching over time in transfected HeLa cells with initial emission rate of 1000 photons per second and molecule (left) and a recording of StayGold and EGFP over three minutes of continuous illumination (16 W/cm²) with recordings every minute (scale bar 20 µm) (right); **b**, mStayGold [21] showing the normalized photobleaching with laser based excitation (1 kW/cm²) of expressed mStayGold in HeLa cells (left), cellular brightness 48 hours after transfection in respect to StayGold including four experiments (center) and respective recordings of cells expressing mEGFP or mStayGold; **c**, mStayGold-E138D [19] depicting the stable protein mutation positions of the monomeric protein (left), percentage of the initial brightness of the fluorescent proteins after fusion with human tropomyosin2 in fixed human RPE-1 cells (7.4 W/cm²) (center) and respective recordings before and after a 600 second waiting time (scale bar 10 µm) (right); **d**, mBaoJin characterization [21] showing the photobleaching curves of all variants compared to conventional fluorescent proteins in live HEK cells under wide-field illumination (5 W/cm²) (left), long term super resolution confocal microscopy images expressing α-tubulin and β-actin after 60 minutes recording time (scale bar 1 µm) (center) and the respective photobleaching curves for different excitation energies (right).

live-cell imaging. These findings were also shown in a more controlled environment of oil droplets ([22] Supplementary Fig. 12). They also investigated the mBaoJin performance using super-resolution confocal microscopy, showing a 20 percent increased photostability in mBaoJin compared to mNeonGreen.
A recent preprint by Ando, Hirano, and collaborators [23] presents a comparative study of the monomeric variants, where each variant was expressed in E. coli and HeLa cells, demonstrating significantly improved bulk photostability and cellular brightness for their variant mStayGold compared to mBaoJin and mStayGold-E138D (Table 1.1). Even more recently, the group of Hirano et al. [25] showed the enhanced cellular brightness and photostability of mStayGold compared to mEGFP in living and fixed HeLa cells employing a range of imaging modalities, including wide-field microscopy, spinning disc multi-beam LSCM, and single-beam LSCM.
In all current studies, the photobleaching and brightness analyses of the mStayGold variants were performed using various excitation methods, where the resulting fluorescence emission signals were integrated across whole cells. Zhang et al. [22] were the first to demonstrate that mBaoJin is suitable for single-molecule applications by using bleaching/blinking-assisted localization microscopy (BaLM) measurements, a method providing all benefits of other SMLM techniques without the need for photo-switchable fluorophores. They measured the photostability in vimentin-mBaoJin transfected live HeLa cells and compared it to mNeonGreen. While the increased photostability of mBaoJin was shown under continuous low-intensity illumination, at high intensities (475–1800 W/cm^2), mBaoJin exhibited photostability comparable to but not greater than mNeonGreen. A recent preprint by Viola et al. [26] investigated the labeling of nanocages carrying sixty fluorescent proteins to determine the intensity and photostability of the variants. While providing additional insights into the properties in that specific application of multiple fluorophores on one label, it also falls short of single-molecule characterization.
While the improved photostability of the mStayGold variants compared to other conventional fluorescent proteins is well established in the works above, their true single-molecule performance characterization and a comparison between the variants have not been done yet.

1.3 Model system for characterization

Characterizing single molecules in a controlled manner requires a model system to simulate a simplified cellular environment and allow unrestricted fluorophore movement within a well-defined platform. A widely used method are decorated supported lipid bilayers (SLBs). The SLBs are constructed of phospholipid molecules, which arrange their hydrophobic tails facing inward and their hydrophilic heads outward, creating a stable bilayer and mimicking a cellular membrane. One side of the bilayer is exposed to an aqueous buffer environment, while the other is facing the solid glass substrate. The mobility and spatial arrangement of lipids within a bilayer are defined by their phase state. A transition between fluid-phase (liquid-disordered phase) and gel-phase (solid-ordered phase) occurs at the phase transition temperature T_M (Figure 1.6) and is highly dependent on physical conditions including pressure or solvent pH. In the gel-phase, hydrocarbon lipid chains adopt an all-trans configuration, leading to complete elongation. This arrangement creates a very compact and ordered lipid network, resulting in a significant reduction in lateral diffusion [27].

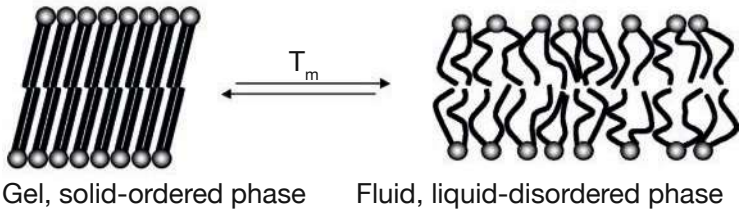

FIGURE 1.6: Illustration of the physical states, gel or fluid, of supported lipid bilayers including the phase transition temperature T_M [27].

Investigating specific experimental settings, SLBs can be functionalized with additional protagonists such as proteins, functional molecules, or antigens (Figure 1.7). This allows for precise customization for experimental needs. However, there are limited possibilities available for integrating recombinant fluorescent proteins into SLBs with controlled orientation while maintaining lateral fluidity [28]. One established solution, introduced in 1988 by Hochuli et al. [29], uses the strong affinity between nickel-chelating lipids (DGS-NTA(Ni)) and polyhistidine-tags, to attach the proteins to the SLB. The DGS-NTA(Ni) groups are implemented in the SLBs, and his-tags are engineered into proteins, building stable and biologically active two-dimensional surfaces. This process is well established in the research group for the anchoring of proteins to study T-cell activation [30].

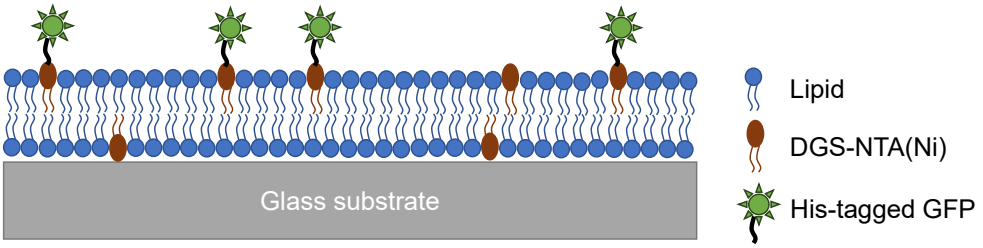

FIGURE 1.7: A concept drawing of supported lipid bilayers and the his-tagged protein attachment.

Visualizing independent single fluorescent proteins on measurement regions spanning several micrometers requires extremely low protein densities. At the same time, labeling densities must remain sufficiently high to achieve statistical significance in the experiment.
Processing starts with detecting fluorescence signals in each frame captured by the camera and assigning each bright spot a precise position and intensity value. These signals must then be tracked across all frames, allowing for the construction of movement trajectories for individual molecules. However, this process presents several complex challenges. Molecules on mobile lipid bilayers may move partially or fully out of the region of interest, interrupting their trajectories. Also, all fluorescent proteins exhibit random blinking between fluorescent and non-fluorescent states. Both of these factors lead to detection gaps, requiring advanced algorithms to link fragmented signals and ensure the trajectory continuity. The brightness of the active fluorophores is also variable, typically exhibiting a broad distribution of intensity. Low-brightness signals can be hard to distinguish from background noise, which may require adjustments within each experiment depending on the overall brightness of the recordings. Various software solutions have been developed today to quantitatively account for blinking behavior, overcounting and related issues in single-molecule recordings [31] or to directly extract reaction rates, diffusion coefficients,

or spatial distributions of bio-molecules in living cells [32]. Yet, given the diversity of single-molecule applications and data sets, every application or even individual experiments often require manual adjustments to optimize localization and analysis.

1.4 Aim of the work

This work aims to evaluate the suitability of the newly developed fluorescent protein mStayGold and all currently developed variants (mStayGold, mStayGold-E138D, and mBaoJin) for single-molecule applications and compare them to conventional mEGFP. For optimal performance in such applications, the key characteristics looked for in mStayGold are high brightness to maximize signal-to-noise ratio and strong photostability for extended tracking of molecular movement. A model setup was established, designed to minimize external disturbances for precise single-molecule measurements. Different software approaches were used to analyze and quantify various aspects of the mStayGold blinking behavior and minimize errors from the algorithm. An extensive examination of single-molecule properties includes metrics on brightness, photostability and blinking patterns to assess the overall performance of the proteins in single-molecule applications. Additionally, the investigation of the impact of several experimental variables, including laser intensity-dependent photobleaching, the effects of mobile versus immobile fluorescent proteins and also comparisons to bulk measurements, are crucial. This comprehensive approach will allow us to make precise and reliable conclusions on the performance of the mStayGold variants in single-molecule applications.
Further, we aim to enhance photostability without requiring additional hardware by introducing stroboscopic illumination. The performance increase will be assessed across the mStayGold variants and with respect to mEGFP.

Chapter 2

Methods

2.1 Bilayer preparation

In this work, two distinct bilayer systems were established. First, mobile bilayers were employed to visualize proteins with two degrees of lateral movement within the membrane plane. Secondly, immobile bilayers were utilized to provide a stable platform for enhanced visualization and error-minimized tracking of single molecules.

2.1.1 Mobile bilayer

The stock solution for mobile bilayers was produced as 1 ml of 125 µM vesicle solution in DPBS(10x) (D1408, Sigma-Aldrich) in fivefold concentration. The solution was composed of 98% DOPC (1-palmitoyl-2-oleoyl-glycero-3-phosphocholine from Avanti Polar Lipids, Inc.) and 2% DGS-NTA(Ni) (1,2-dioleoyl-sn-glycero-3-[(N-(5-amino-1-carboxypentyl)imino-diacetic acid) succinyl] from Avanti Polar Lipids, Inc.). Using DOPC with a molecular weight of 760.076 g/mol at a concentration of 10 mg/ml in chloroform and DGS-NTA-Ni with a molecular weight of 1055.513 g/mol at a concentration of 1 mg/ml in chloroform, the necessary volumes were calculated as 46.5 µl of DOPC and 13.2 µl of DGS-NTA-Ni. These two components were poured in a glass vial and evaporated under a stream of nitrogen while continuously spinning the glass, resulting in a film forming on the walls. To ensure complete evaporation, an additional nitrogen flow was applied over 10 minutes. Subsequently, 1 ml of DPBS(10x) was added into the vial and the mixture was vortexed (IKA Labortechnik) until it became milky. The solution was then treated in an ultrasound bath for 10 minutes until it became clear again. The resulting vesicle solution can be stored or used directly for bilayer preparation.

Next, a microscope coverslip (Menzel-Gläser, 24 x 60 x 1.5 mm) was plasma cleaned (Harrick Plasma) for 10 minutes to clean the surface and make it hydrophilic to achieve sufficient spreading of the vesicle solution. After cleaning, the coverslip was glued to a clean Lab-Tek chamber (Nunc, Lab-Tek, 8 chambers on coverglass) using a bio-compatible two-component adhesive. The fivefold concentrated vesicle solution was diluted with 10x DPBS before being added into the wells of the Lab-Tek chamber, where it should cover the hydrophilic glass surface nicely. Subsequently, the chambers were incubated at room temperature for 20 minutes. After 20 minutes, the bilayer had formed on the glass and the wells got washed with 15 ml of 1x DPBS (D8537, Sigma-Aldrich). Finally, the meniscus of the filled chambers was removed, and 330 µl of DPBS was extracted to maintain uniform filling levels in the wells.

2.1.2 Immobile bilayer

The preparation of immobile bilayers followed a procedure similar to the process in Section 2.1 with some key modifications. Firstly, DPPC lipids (1-palmitoyl-2-docosahexaenoyl-sn-glycero-3-phosphocholine from Avanti Polar Lipids, Inc.) were used instead of DOPC. The phase transition temperature T_M is 41 °C for DPPC. For reaching the solid-ordered gel phase, the lipids have to be treated with a temperature above T_M. Therefore, the water temperature of the ultrasound bath when treating the vesicle solution was heated to 55 °C. Also, the incubation of the bilayer in the Lab-Tek Chambers was performed at 55 °C for 20 minutes in an incubator.

2.2 Proteins

After formation of a homogeneous mobile or immobile bilayer, the proteins of interest can be added. The proteins used in this study were produced by M.Sc. Lucia Cikatricisová under the supervision of Prof. Ario de Marco from the University of Nova Gorica. The stock samples included mStayGold (3.25 mg/ml in PBS + 5% glycerol at pH 7.4), mStayGold-E138D (2.44 mg/ml in PBS + 5% glycerol at pH 8.0), mBaoJin (2.11 mg/ml in PBS + 10% glycerol at pH 7.4) and conventional mEGFP (1.94 mg/ml in PBS + 10% glycerol at pH 7.4). The amount of protein used in the experiments ranged from 0.001 ng to 40 ng per well, depending on whether single-molecule or bulk measurements were performed. Especially in single-molecule experiments, it is crucial to maintain a density low enough to resolve individual molecules while ensuring sufficient signals for statistical analysis. The densities were determined experimentally, resulting in amounts of protein per well for single-molecule measurements of e.g., 0.02 ng (mEGFP), 0.02 ng (mSG-E138D), 0.005 ng (mBaoJin) and 0.01 ng (mStayGold) in the results below. The selected amount of protein was diluted in 50 µl of DPBS(1x) per well before adding. The solution has to be pipetted very carefully because the bilayer on the bottom of the well is very sensitive to touch and would be destroyed if the pipette tip scratches it. Also, touching of air bubbles would lead to immediate dissociation of the lipid bilayer. Following this, the wells were incubated for 60 minutes. During the handling of protein-labeled samples, it is crucial that the Lab-Tek chamber is protected from direct light to prevent premature photobleaching. After incubation, the wells were washed with 15 ml of DPBS(1x) and the meniscus as well as 330 µl of the buffer were carefully removed to maintain uniform filling levels.

2.3 Experimental microscopy setup

The prepared wells were placed in the sample holder of the microscope (Zeiss Axiovert 200(M)). Fluorescent protein excitation was achieved using a blue 488 nanometer laser from an Oxxius L6Cc RGB laserbox operating at 150 mW. The laser parameters were adjusted using the manufacturer's software, *Oxxius Lasers*. The laser beam was directed through a series of mirrors, lenses and an aperture on the optical table and subsequently directed into the microscope (Figure 2.1). The appropriate TIRF angle was adjusted by shifting the stage of the mirror, shifting the beam parallel into the microscope and changing the TIRF angle in the objective. The microscope included an immersion oil (Carl Zeiss Immersionoil 518 F) objective (100x Zeiss αPlan-Apochromat, 1.45 NA) and a tube lens with 1x magnification. A dichrioc mirror (CHROMA zt488/640rpc) was employed and the specific wavelengths allowed to

pass to the camera are additionally limited through a dual-bandpass filter (Semrock FF01-538/685-25). The resulting signals from the samples were recorded using an iXon EMCCD camera (Oxford Instruments). Ensuring that all recordings remained in focus, particularly when covering larger sample areas or to avoid time drift during extended measurement periods, a focus-hold system is crucial. This system operates by directing an infrared diode beam onto the sample and reading the back-reflected beam using a detector, as shown in Figure 2.1. A change in the z-axis of the object directly causes a shift of the back-reflected beam in the x/y direction on the detector plane. An in-house software, coupled with a PID controller and a piezo-controlled objective, maintained a constant focal plane throughout the experiments.

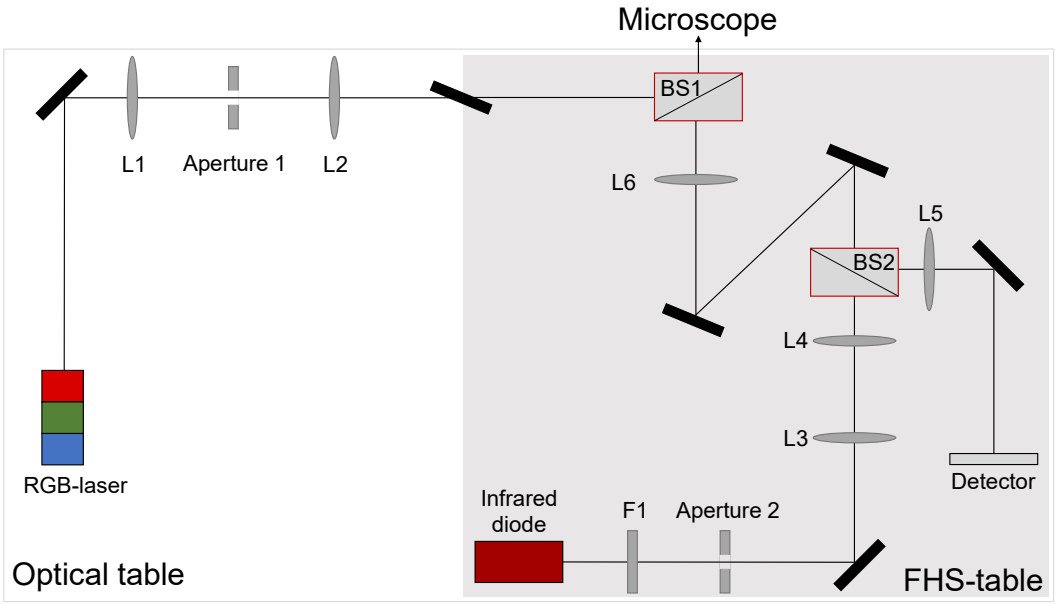

FIGURE 2.1: The TIRF microscopy table setup, where the white area represents the optical table with the RGB laser optics that are directed towards the microscope via a beam splitter (BS1), where the infrared signal from the focus-hold table (gray area) is added. (Lx): lenses, (Fx): filter, (BSx): beam splitter

The communication between the laserbox, camera and TIRF-stage was facilitated through an in-house software *sdt-control*, a LabVIEW-based GUI, in combination with an NI DAQ card (National Instruments) for communication. The software allows for independent modulation of the RGB lasers, the respective shutters, the camera trigger and the camera shutter, making complicated sequences possible to generate various illumination patterns. The TIRF angle was adjusted and stored in an additional in-house GUI called *servotisch*. To account for fluctuations of the laser beam angle between experimental sessions, the TIRF angle was adjusted and stored in every experiment to maximize fluorophore signal output and minimize background noise.
At the start of the measurement procedure, the voltage for the laser modulation was set to be between 0 and 5 V. The camera was cooled to -60 °C and the linear electron-multiplying gain (EM-gain) was adjusted based on the sample brightness to achieve a sufficient amount of counts on the camera without reaching saturation of 50,000. In this work, an EM-gain of 300 was used in all experiments. This gain factor must be considered when recalculating the actual photon emission from the recorded data (Equation 2.2). Since the actual laser intensity at the probe may vary depending on

the laser aperture opening and ambient fluctuations, the laser intensity at the objective was measured before each experiment. Therefore, a dummy probe was placed on the measurement stage, the laser field stop was adjusted and the illuminated area on the camera was measured in pixels using the camera. Subsequently, a digital power meter (Thorlabs, Inc.) was positioned on the objective to measure the actual laser intensity. The pixel size of the camera (0.16 µm/px or 0.16 x 10^{-4} cm/px), the illuminated area ($A_{measured}$) in px^2 and the measured intensity at 488 nm ($I_{tot\_measured}$) in Watts were then used to calculate the laser intensity in W/cm² (Equation 2.1).

$$I_{laser} = \frac{I_{tot\_measured}}{A_{measured} \cdot (0.16 \cdot 10^{-}4)^2} \tag{2.1}$$

The readout time of the camera is dependent on the horizontal and vertical readout speed of the region of interest (ROI). The selected ROI defines the total readout speed of each image. The delay time between consecutive frames and the shutter delay time were adjusted accordingly. In these experiments, the ROI was configured to be read out faster than 10 ms and the delay time was set to be 10 ms between each recording. A total of 300 images were recorded per position and the illumination time ranged between 1 and 80 ms, depending on the experimental requirements. The laser intensity for each experiment was set by adjusting the attenuation value in the *sdt-control* software.

Stroboscopic illumination

In this approach, the continuous illumination of five milliseconds per image was chopped into 2500 bursts of two microseconds. This method ensured comparability to conventional illumination by maintaining the same overall light dose per image (Figure 2.2). Additionally, a time delay of either two or four microseconds between the two microsecond pulses was introduced to explore the potential impact of the prolonged resting time and resulting total measurement period (t_{pulses}) on the photostability of the fluorescent protein.

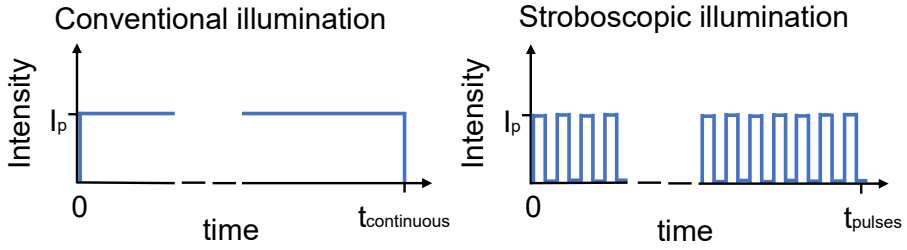

FIGURE 2.2: Excitation laser intensity for continuous illumination of one image (left) compared to stroboscopic illumination (right).

The stroboscopic illumination sequence was programmed using a custom Python script. The *sdt-control* software controls the lasers, shutters and camera by sending the on/off command of eight channels, represented by an 8-bit code of 1/0, simultaneously to the communication card for each grid increment (2 µs). The bits represented the following commands: Bit 1: red laser, Bit 2: green laser, Bit 3: blue laser, Bit 4: camera trigger, Bit 5: red laser shutter, Bit 6: green laser shutter, Bit 7: blue laser shutter and Bit 8: camera shutter. The Python script constructed a *.txt* file containing the sequence of these 8-bit commands depending on all steps in one experiment after inserting the experimental settings, including the grid time (2 µs), pulse up-time

(2 µs), pulse down-time (2 or 4 µs), number of pulses (2500) and the laser channel (blue). The *.txt* file was then uploaded into the *sdt-control* software.

2.4 Data processing

Bulk data processing

The recorded image sequences require further advanced analysis before conclusions on the quality of the fluorescent proteins can be drawn. As an initial step, the recordings were processed using a Python package called *sdt-python* [33], which was developed within the research group. This package provides a comprehensive collection of tools for the analysis of fluorescence microscopy data, including the evaluation of brightness data, multi-color datasets, ROI handling, GUI for the localization of fluorescent features, or analysis of localization data. After setting parameters for frame rate, pixel size and exposure time, the brightness for each bulk recording was analyzed and compared by subtracting the corresponding background signal. By selecting an appropriate ROI in the center of the laser intensity maximum, where the photobleaching is strongest, the photobleaching curves can be determined. Single-molecule localization, in contrast, requires more sophisticated data analysis techniques.

Single-molecule data processing

In this study, two localization approaches, *DaoSTORM* combined with *Trackpy* and *ThunderSTORM* combined with a MATLAB script, were utilized to create a comprehensive result by investigating and mitigating potential errors or misinterpretations from the localization algorithms themselves. Both approaches follow the same principle (Figure 2.3). Initially, filters are applied to localize the fluorescent proteins in each individual frame. Subsequently, the frames are stacked to track movement patterns and measure time-dependent brightness. The resulting brightness profiles are then analyzed using statistical approaches.

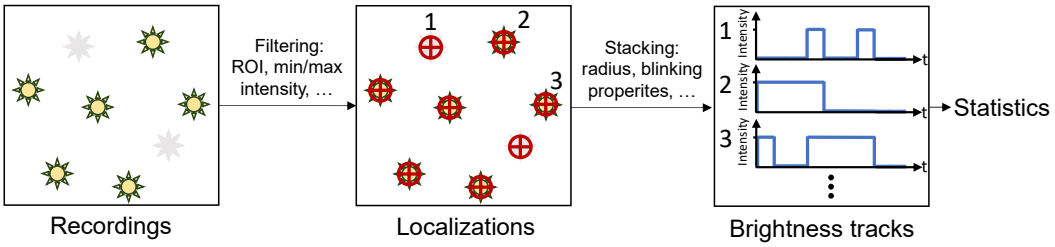

FIGURE 2.3: Single-molecule data processing concept.

2.4.1 DaoSTORM + Trackpy

The *DaoSTORM* algorithm [34] is used as a Python plugin in *sdt-python* [33], which is using *trackpy* [35] for further analysis of the localization datasets. The *DaoSTORM* algorithm is employed to localize the on-times of the blinking fluorescent proteins and their integrated single-molecule brightness. The model requires several parameters to be optimized for accurate signal recognition, including the expected localization radius in pixels (2 pixels), model type (2-dimensional), ROI, starting frame (0), filter type (Gaussian), minimum distance between two localizations (2 pixels) and the

size range for fitting of a Gaussian curve (0.6 to 1.4). The threshold is manually adjusted depending on the overall brightness of the fluorescent proteins of interest to ensure that all brightness fluctuations of a fluorescent protein are recognized as localizations while background signals are excluded. The resulting data consists of the position (x, y) and the mass (brightness measured as area under Gaussian fit in counts) of each individual localized signal for every recording and frame.
Subsequently, *Trackpy* is used to stack the images and compute various statistics for the individual particles, such as particle count, lenROI (number of consecutive localizations for a single particle inside the ROI), background brightness and frame number of localizations. In the *sdt-python* plugin, the maximum number of times a particle can be localized at the same position and still be counted as a particle has to be defined according to the bilayer fluidity. A lower value (15) is used to exclude immobile particles in fluid bilayers or a higher value (300) is used to account for fluorescent proteins in immobile bilayers. In this study, we used the mass to calculate the single-molecule brightness and the lenROI value as the on-time of the fluorescent proteins. In the data analysis, localization lengths of one are excluded for all experiments as they collect all misinterpreted noise as signals. At this point, the single-molecule brightness was still expressed as counts measured by the camera. To calculate the brightness in actual number of photons emitted, it is necessary to account for the camera specifications, including the conversion factor of photoelectrons per $A/D_{\text{conversion}}$ unit (15.7) and the EM-gain (300) (Equation 2.2).

$$\text{brightness [photons]} = \frac{\text{brightness [counts]} \cdot A/D_{\text{conversion}}}{\text{EM-gain}} \tag{2.2}$$

2.4.2 ThunderSTORM + MATLAB

The second approach employed the *ThunderSTORM* algorithm [36], an open-source ImageJ plugin. The resulting data was further analyzed using a MATLAB script that was developed and published by the research group [31]. While the *ThunderSTORM* algorithm is used for localizing the signals similarly to the previously described approach, it offers additional useful settings for more sophisticated analysis. The parameters to insert include image filtering (Wavelet filter, B-Spline order = 3, B-Spline scale 2.0) and the sub-pixel localization of molecules (Method = Gaussian, fitting radius = 3 px, fitting method = Weighted least squares, initial sigma = 1.6 px). As with the prior method, threshold values for localization must be adjusted individually based on the total experimental brightness and background. The *ThunderSTORM* algorithm includes a feature where the peak brightness threshold is adjusted automatically depending on the standard deviation of the first wavelet level of the recording, correlating directly to the noise in the image. For this study, the minimum brightness threshold was empirically set to three times this standard deviation (3*std(Wave.F1), method = local maximum). Additionally, camera setup parameters such as the conversion factor of photoelectrons per $A/D_{\text{conversion}}$ unit (15.7), EM-gain (300) and pixel size (160 nm) can be inserted directly. As a result, the brightness values for the single molecules are automatically calculated in photon units. Although the *ThunderSTORM* algorithm would allow for additional filtering and stacking, the MATLAB script developed by the group was employed to maintain full control over the analysis process. To efficiently analyze a large number of recordings, a macro was used in ImageJ to insert all parameters from above and restrict the recordings to a specific ROI. The ROI application in this initial step is reducing the processing time considerably by minimizing the localization effort to the relevant regions. The

output of the *ThunderSTORM* algorithm is stored as individual *.CSV* files for each recording, where x-position, y-position, sigma, brightness (photons), offset, bkgstd and uncertainty are stored for each localization.
As the MATLAB script was initially developed for two-color co-analysis of clustered blinking data, the *platform_correlation* was disabled in the *run_analyseBlinkStat* code to include only single datasets without co-localization. Running the main program (*main_analyseBlinkStat*) for collecting the *.CSV* files containing the localization data for each experiment and setting individually, several parameters were set, including distance metric (euclidean), linkage criterion (average), criterion for defining clusters (distance) and cutoff (200). In the next step, a manually drawn ROI was asked from the script. Since the ROI was already specified in the macro execution, the entire region was selected here. The script is then stacking the images from each recording and linking the localizations to track particles throughout the images of a recording. The resulting output distributions include the on-times (number of consecutive frames that the fluorescent label is in its bright state), off-times (number of consecutive frames that the fluorescent label is in its dark state), number of localizations (total number of detections of an individual fluorescent label), number of gaps (number of gaps between detection burst sequences), number of bursts (number of consecutive bursts of one individual label) and the start frame (frame number of first appearance of individual fluorescent label). Among these, the on-time, off-time, number of localizations and number of gaps were found to be sufficient for a comprehensive analysis of the blinking behavior of fluorescent proteins. The resulting distributions were stored in *.mat* files, which were processed further using a Python script. During subsequent data analysis, all localizations with length one were excluded, as with the *DaoSTORM* algorithm approach.

2.4.3 Further calculations

Single-molecule photobleaching probability

To visualize similarities of the bulk photobleaching curves and the single-molecule photobleaching data, a SM-photobleaching curve was calculated from the SM-data by developing a Python based approach (Figure 2.4).

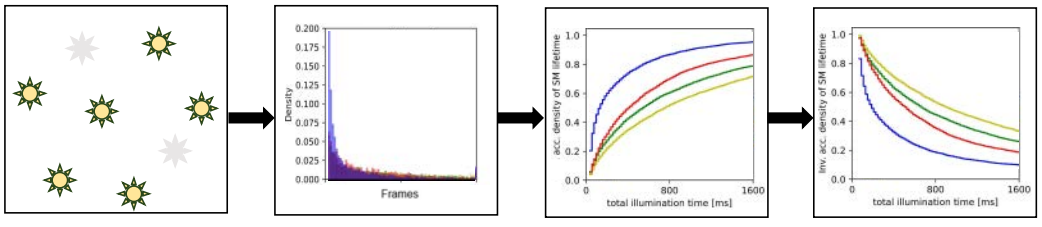

FIGURE 2.4: The concept of the single-molecule photobleaching curve development.

After localization of the single molecules, the distributions of number of localizations over frames in the data were extracted. Then a histogram over time was produced using the illumination time setting per frame to calculate the total illumination time on the x-axis. The resulting histogram shows the fraction of particles that lasted until a specific time point. Cumulating the fractions and inverting the curve results in the photobleaching probability over time for single molecules results in the same information as the photobleaching curves from bulk measurements.

Bi-exponential decay estimation

The performance quantification of photobleaching curves (bulk or single-molecule) was done using bi-exponential decay estimation (Equation 2.3) and calculation of a mean lifetime $T_{W1/2}$ (Equation 2.4). The decay estimation was carried out using the *curve_fit* function from the *scipy.optimize* Python package. The initial parameter estimation for c, T_1 and T_2 were set as 0, 100 and 100, respectively. For further validation of the results, the half-life $t_{1/2}$, where the raw data reaches half of the initial value, was also determined for each measurement (Equation 2.5).

$$y(t) = c \cdot e^{-t/T_1} + (1 - c) \cdot e^{-t/T_2} \tag{2.3}$$

$$T_{W1/2} = \frac{c \cdot T_1 + (1 - c) \cdot T_2}{2} \tag{2.4}$$

$$t_{1/2} = T_{W1/2} * ln(2) \tag{2.5}$$

Protein density calculation

The number of fluorescent proteins per area in bulk images was calculated by dividing the total integrated brightness of the first image of a recording by the single molecule-brightness of the corresponding fluorescent protein at the same laser intensity in a specific ROI. The number of fluorescent proteins is then divided by the ROI-area A_{ROI} that is calculated from the pixel size in µm to receive a density in molecules/µm². When different illumination times were used across datasets, the single-molecule brightness was extrapolated to for the calculation.

$$\text{density} = \frac{\text{total integrated brightness}}{\text{single-molecule brightness}} \cdot \frac{1}{A_{ROI}} \tag{2.6}$$

Chapter 3

Results and Discussion

The three monomeric StayGold variants (mSG-E138D, mBaoJin and mStayGold) are hypothesized to exhibit strong improvements in single-molecule brightness and photostability compared to conventional fluorescent proteins like monomeric EGFP (mEGFP). In this thesis, the goal was to identify the brightest and most stable proteins that are best suited for fluorescence microscopy applications. To achieve a comprehensive characterization, the fluorescent proteins' behavior was examined from multiple perspectives. Initially, the proteins were anchored on fluid bilayers at high densities to assess their bulk photobleaching behavior. Subsequently, the protein density was reduced to allow for the independent characterization of single molecules. Their characteristic photobleaching and brightness patterns are determined using two individual localization algorithms and various experimental approaches, including intensity-dependent excitation, characterization on both mobile and immobile bilayers and a direct relation between bulk and single-molecule results. Additionally, an attempt is made to further prolong the lifetime of the fluorescent proteins using stroboscopic illumination, an advanced excitation technique that is easy to implement and does not require additional hardware.

3.1 Bulk photobleaching

The first approach for the assessment of the photostability was the investigation of densely labeled fluorescent proteins on mobile SLBs and excitation with the 488 nm laser for measuring bulk signals. The resulting recordings of the respective proteins, conducted with a laser intensity of 513.6 W/cm², showed distinct photobleaching after recording of 200 images, each with 5 ms illumination time, resulting in 1000 ms of total excitation time (Figure 3.1a). Despite aiming for a constant protein density, fluctuations were observed. The density calculations revealed 2.9 ± 0.7 molecules/µm² for mEGFP, 8.6 ± 1.9 molecules/µm² for mSG-ED, 18.9 ± 5.3 molecules/µm² for mBaoJin, and 6.1 ± 1.46 molecules/µm² for mStayGold. This indicates that mEGFP had the lowest density, while mBaoJin had a much higher density. Additionally, mEGFP proteins completely photobleached after 1000 ms of illumination, whereas mStayGold protein variants remained clearly visible under the same contrast settings. Conversely, the mBaoJin samples, despite having the highest density, exhibited lower brightness in the laser center compared to the other two variants after 1000 ms of illumination. For correct quantification of the bulk photobleaching results, the mean brightness inside the region of interest (ROI) was measured across all 300 images and normalized by the initial brightness of the first image. For all four protein types, five positions were recorded per laser intensity setting, yielding in the photobleaching curves for the respective recordings (Figure 3.1b). By maintaining a constant illumination time and repeating the experiment with different excitation intensities, a direct correlation between photobleaching and laser intensity can be

observed in the bleaching curves. The position and size of the ROI used for the calculation influences the results of the photobleaching curves. Firstly, because of the Gaussian shape of the incoming laser beam, the center of the ROI had to be aligned with the center of the laser maximum to achieve photobleaching as uniformly distributed as possible inside the ROI. Secondly, the size of the ROI has to be chosen small to minimize the intensity fluctuations from the Gauss shape of the incoming beam and to avoid rediffusion of partly photobleached fluorescent proteins from the border regions while being sufficiently large enough to collect enough fluorescence signal. Supportive of this, the laser field stop was opened, resulting in a large photobleaching area.

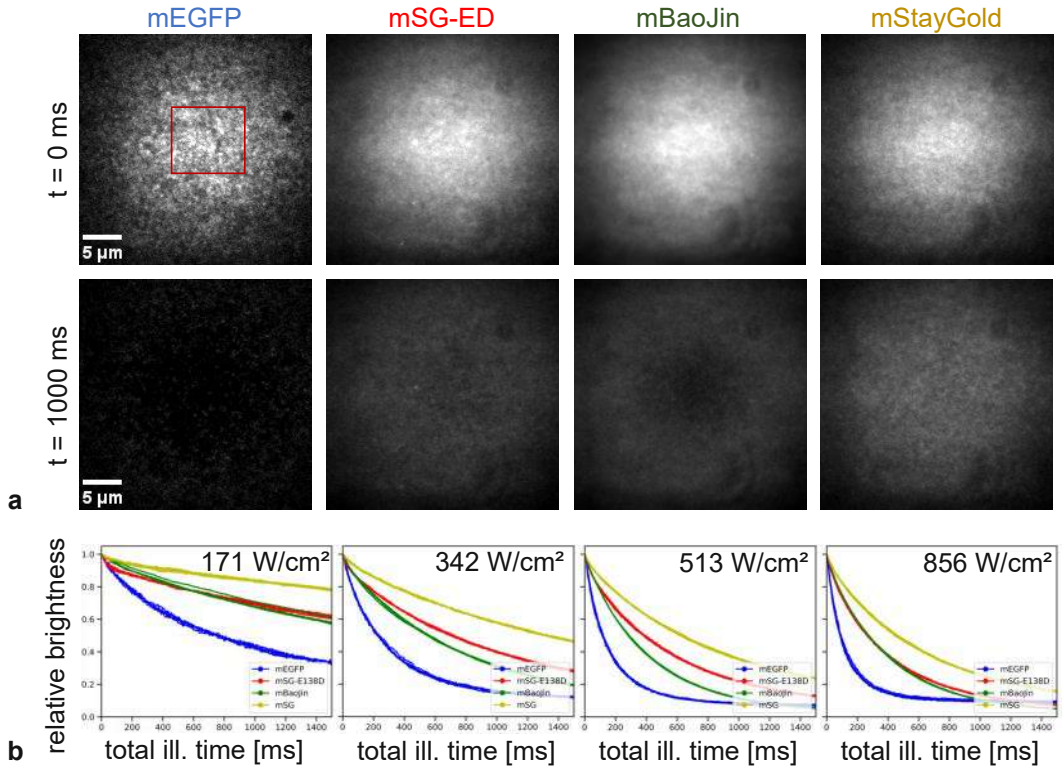

FIGURE 3.1: The results from the bulk recordings of the four fluorescent proteins: **a**, an example of a mobile SLBs at one position each with 513 W/cm² laser intensity and 5 ms illumination time. The top row shows the first images at t = 0 ms and the bottom row shows the respective positions after 200 images, equal to a total illumination time of t = 1000 ms. The red rectangle is representing the ROI for the calculation of the photobleaching curves. **b**, the photobleaching curves of bulk samples showing the normalized brightness in respect to the total illumination time, including five measured curves at different positions on the SLB per protein and four different laser intensities for EGFP (blue), mStayGold-E138D (red), mBaoJin (green) and mStayGold (yellow).

For further quantification of the data, the photostability of the fluorescent proteins was determined by fitting a bi-exponential decay function to the data and subsequent calculation of the halftime (Chapter 2.4.3). The fits for the curves in Figure 3.1 are shown in Figure A.1, demonstrating strong similarities of the fit and the data. For each of the five individual measurements per setting, the mean halftime as well as the overall mean across two individual experiments was calculated (Figure 3.2). Since the actual laser intensities measured in the experiments deviated from the expected 150, 300, 600 and 900 W/cm², the values displayed in Figure 3.2 represent the mean value of the two intensities measured in each experiment. The bulk halftimes

were significantly higher for mStayGold compared to the other two variants and mEGFP for both experiments and at all laser intensities measured. The total mean halftime increase for mStayGold compared to mEGFP resulted in +840%, +530%, +330% and +185% for increasing laser intensities. Both other mStayGold variants also demonstrated improved photostability compared to mEGFP (mBaoJin: +475%, +270%, +166%, +117%; mSG-ED: +260%, +245%, +192%, +118%), but their photostability remained inferior to that of mStayGold.
A direct comparison of the photobleaching half-life values reported here to the previously published data is not feasible as the excitation intensities for the bulk measurements there were several magnitudes lower than those employed in this work and the experimental approaches differed substantially. Ando et al. [21] conducted an experiment that most closely aligns with the conditions of this work, using mStayGold expressed in HeLa cells and a laser excitation intensity of 1 kW/cm². In that experiment, they observed a 5-fold increase (+400%) in half-life compared to mEGFP (Figure 1.5b). Although the experimental conditions differed significantly, the relative change in the half-life of mStayGold compared to mEGFP reported by Ando et al. falls within a similar range as the results presented in this study.

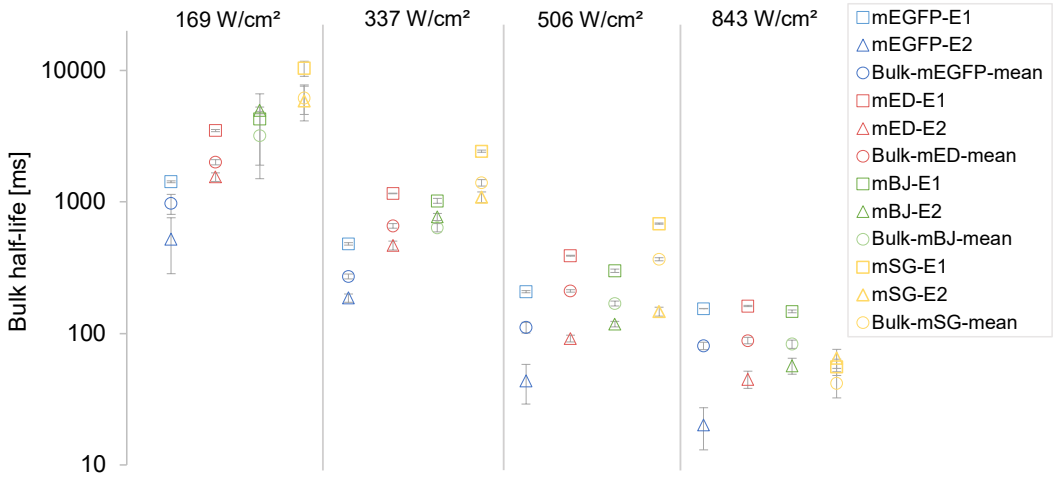

FIGURE 3.2: Logarithmic half-life mean value for two individual bulk experiments (E1, E2) including five measurement positions per experiment over four laser intensities in each experiment.

In the photobleaching curves presented above (Figure 3.1), the recordings were normalized to the initial brightness. However, the absolute brightnesses of the samples vary between samples because of density fluctuations resulting from deviations in the dilution in the preparation, varying number of active fluorescent proteins or deviations in stock concentrations. The resulting differences in photostability measured from the bulk photobleaching curves that were interpreted as variations in protein brightnesses could also directly result from those density variations. For correctly assessing the brightness of the fluorescent proteins and determining the true photostability by investigation of the blinking behavior, single-molecule measurements have to be performed.

3.2 Single-molecule measurement

Ensuring that individual molecules were visible and trackable in the single-molecule measurements, the sample density was subsequently reduced. The optimum dilutions had to be found experimentally by recording images for different dilution steps. An example recording for each of the four proteins on immobile bilayers in one experiment is shown in Figure 3.3 showing the limits of the labeling densities. The mStayGold density is close to exceeding the density limit but is still measurable. The mEGFP or mSG-ED variants show low densities, requiring more recordings to reach a similar number of total localizations for the analysis. Nevertheless, all signals are well separated and bright compared to the background noise and hence optimal for single-molecule analysis.

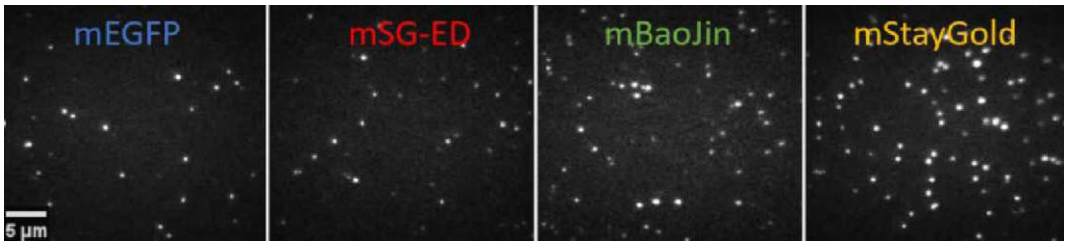

FIGURE 3.3: First image of a single-molecule recording with 331 W/cm² laser intensity and 40 ms illumination time on immobile bilayers under equal contrast settings for all images. The amount of protein per well were 0.1 ng for mEGFP, 0.1 ng for mSG-ED, 0.015 ng for mBaoJin and 0.04 for mStayGold.

The objective of this experiment was to characterize the lifetime and brightness of the fluorescent proteins, focusing on their distinct blinking behavior. Specifically, we aimed to determine how long each of the fluorescent proteins remains active (on-time), how long it remains inactive (off-time), how often it blinks within a fixed measurement period, how often it is detected in total and how bright it is (Figure 3.4a). The brightness of the single fluorescent proteins can vary strongly over time and between proteins (Figure 3.4b). Localizing the brightness profiles over time has to be done carefully to only include single molecules by applying maximum brightness thresholds, maximum size restrictions, minimum distances between neighboring particles and to exclude all background from being localized as a particle by applying a minimum brightness threshold.

In the following single-molecule experiments, the proteins were attached to immobile bilayers, as it simplifies the tracking process of the single molecules by keeping them in a fixed position. While several localization algorithms are available and they should ideally produce similar results, each approach comes with its own methodology, which could lead to slightly different results. To minimize the influence of the tracking algorithm and ensure an accurate characterization of the single molecules, two different algorithms were adapted to match the needs for this work (Chapters 2.4.1 and 2.4.2). Both approaches yield distributions of characteristic single-molecule parameters. One such distribution for the on-times and the single-molecule brightness, derived from the *DaoSTORM* + Python method, is shown in Figure 3.5. The resulting histograms demonstrate broad distributions of on-times and brightness across all localizations and proteins. While the detection frequency of mEGFP and mSG-E138D is higher at lower on-times, the other two variants appear to show a change towards longer on-times. However, a direct comparison based solely on these distributions is challenging. For a more conclusive comparison, box plots describing the distributions were generated and the mean

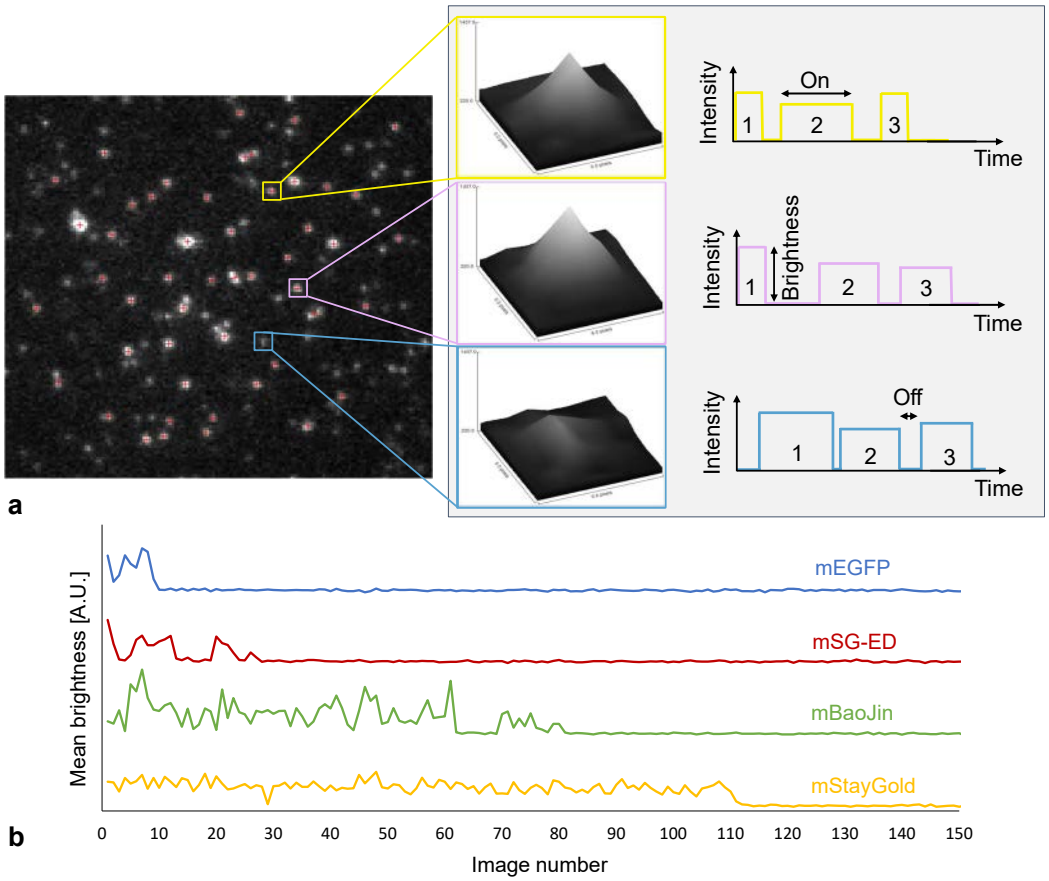

FIGURE 3.4: Single molecule recordings of: **a**, mBaoJin at 1368 W/cm² laser intensity and 5 ms illumination time showing the first image, including the tracked positions (red crosses) from the ThunderSTORM algorithm and three example localizations displaying the 2D-intensity distributions, including an illustration of the time-dependent intensity of an individual protein over a specific time span. **b**, examplary time traces of the single-molecule brightness of one fluorescent protein over time measured using ImageJ in a 6px times 6px area representing one trace per protein measured under identical experimental conditions (1368 W/cm² and 5 ms).

values were calculated for every protein and condition (Appendix A). Comparing the calculated mean values with the distributions, we established that the overall statement can be effectively captured by the mean value and standard deviation. These statistical parameters are used in the results below to represent the distributions. The single-molecule experiments were designed to assess the dependency of illumination time and laser intensity while maintaining a constant total laser dose for the fluorescent proteins. This approach ensures that all settings result in a similar number of photons measured per molecule, minimizing additional effects resulting from detection algorithm efficiencies or possible brightness dependencies in the experimental setup. Starting with the initial intensity of 1200 W/cm² and 10 ms of illumination time, the laser intensity was systematically divided by a factor of two in four steps while the illumination time was correspondingly doubled, resulting in 600 W/cm² and 20 ms, 300 W/cm² and 40 ms, as well as 150 W/cm² and 80 ms. The experiments were repeated independently three times. As with the previous experiments, small variations (<5%) in laser intensity were observed in the three experiments. Therefore, the comparability of the results is given and in this chapter, we depict the defined laser intensity values from above to refer to the respective

setting. The actual measured laser intensities for each setting are depicted in the *ThunderSTORM* + MATLAB section of the Appendix A.

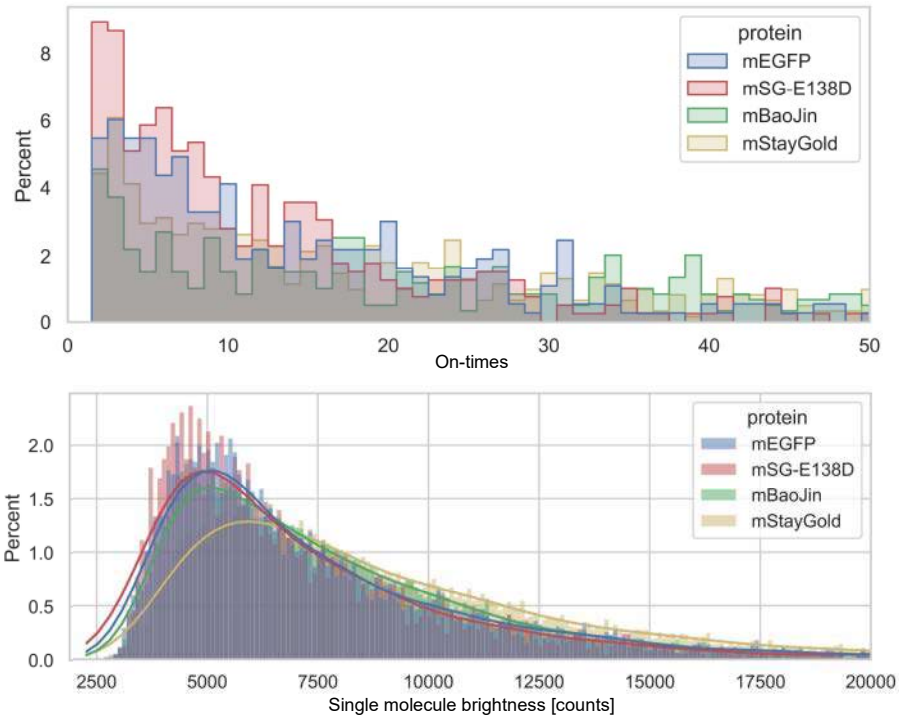

FIGURE 3.5: The distributions of on-times (top) and single-molecule brightness (bottom) for all fluorescent proteins from one experiment at 664 W/cm² and 40 ms illumination time were retrieved from the *DaoSTORM* + Python approach.

3.2.1 Single-molecule Blinking

In the following, the single-molecule parameter results are discussed in detail. The results are displayed in combined graphs where the '-p' values (dark) represent the mean values from each experiment extracted using the *DaoSTORM* + Python approach and the '-m' values (light) using *ThunderSTORM* + MATLAB, respectively. The bars represent the p-mean and m-mean values and the corresponding total standard deviation ($stdev_{tot}$ = sqrt($stdev_1^2$ + $stdev_2^2$ + $stdev_3^2$), combining all data points from all three experiments in the respective setting. The number of positions recorded on a bilayer with a specific protein and laser intensity setting was varied between 10 to 20 recordings, depending on the surface density, to a achieve similar number of localizations across all samples. Overall, 450 individual single molecule recordings were performed and included in the analysis. In total, the Python tracking resulted in 91762 particles analyzed and the MATLAB tracking resulted in 80055, respectively. The two values may vary because of differences in the localization algorithm (thresholds, integration, etc.) or because of differences in the linking approaches and differences in thresholds in the tracking algorithms. The number of values used in the respective blinking parameters per experiment and setting are listed in the raw data distributions in Appendix A.

On-times

The on-times represent the durations of the active states of the blinking fluorescent protein. The on-time was measured in number of frames as the total light dose per frame remained constant while the illumination times and laser intensities vary between settings. The resulting mean on-time values (Figure 3.6) were calculated from the respective distributions (Appendix A displaying the individual raw data box plots for all experiments). The resulting on-time mean values vary within a range of five to twenty frames between experiments, while the standard deviations span much larger regions due to the broad on-time distributions as observed above (Figure 3.5). Nevertheless, the mean values of mBaoJin and mStayGold were higher compared to mEGFP and especially compared to mSG-E138D. As the photobleaching effect increases for increased laser intensities, the overall on-times decrease across all proteins and experiments.

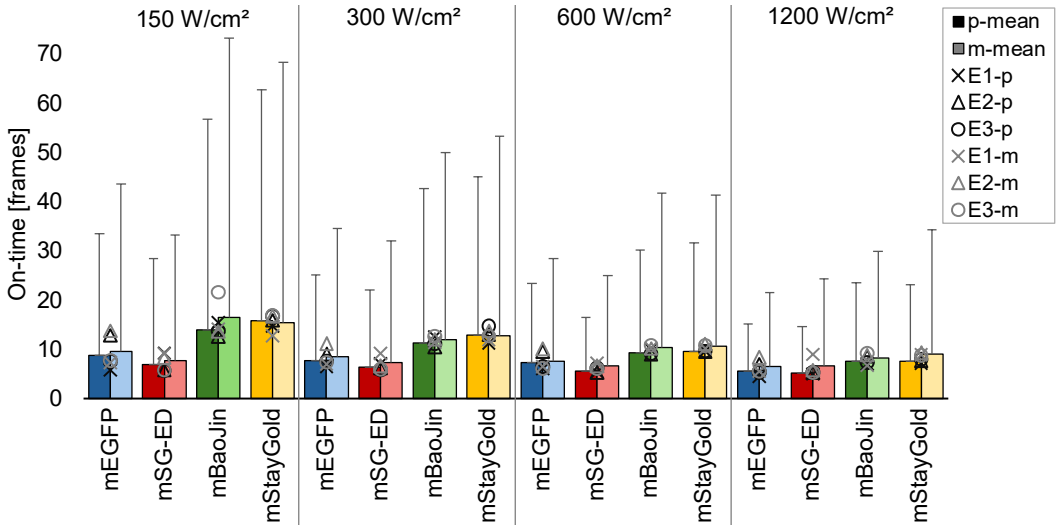

FIGURE 3.6: Resulting single-molecule on-times were measured on immobile lipid bilayers, including the four laser intensity steps (150 W/cm² + 80 ms, 300 W/cm² + 40 ms, 600 W/cm² + 20 ms and 1200 W/cm² + 10 ms). The depicted values include the mean values of the recordings from three independent experiments (E1-E3) and both localization methods (-p and -m). The bars represent the overall mean value of all experiments under each condition, along with the corresponding standard deviation.

To make an assessment on the performance of the mStayGold variants, the relative increase or decrease in mean values in respect to the conventional mEGFP values for each individual experiment was determined (Figure 3.7). Thereby, we account for variations between experiments and directly receive a characteristic change compared to mEGFP. The resulting changes compared to mEGFP showed pronounced longer on-times for mStayGold for all experiments and settings (Figure 3.7). In total, mStayGold showed an increase of +58.0% ± 30.8 for the Python-based method (-p) and +54.6% ± 28.4 for the MATLAB-based method (-m). mBaoJin exhibited a similar increase compared to mEGFP with slightly larger variability, resulting in +52.6% ± 35.9 for (-p) and +53.5% ± 40.1 for (-m). The highest increase of up to 150% was achieved for mStayGold and mBaoJin with the lowest laser intensity and longest illumination times. The intensity dependency here may result directly from the increased total on-times as seen above. In contrast to mStayGold, mSG-E138D did not display a clear trend towards increased on-times compared to mEGFP resulting even in decreased on times with -8.5% ± 45.6 for (-p) and -5.6% ± 29.1 for (-m).

Longer on-times, at this point, already suggest an overall increase in fluorescent output over time. However, due to the characteristic blinking behavior of the fluorescent proteins, this increase may not necessarily indicate longer lifetimes, as it could also result from a decrease in off-times while the total lifetime remains constant.

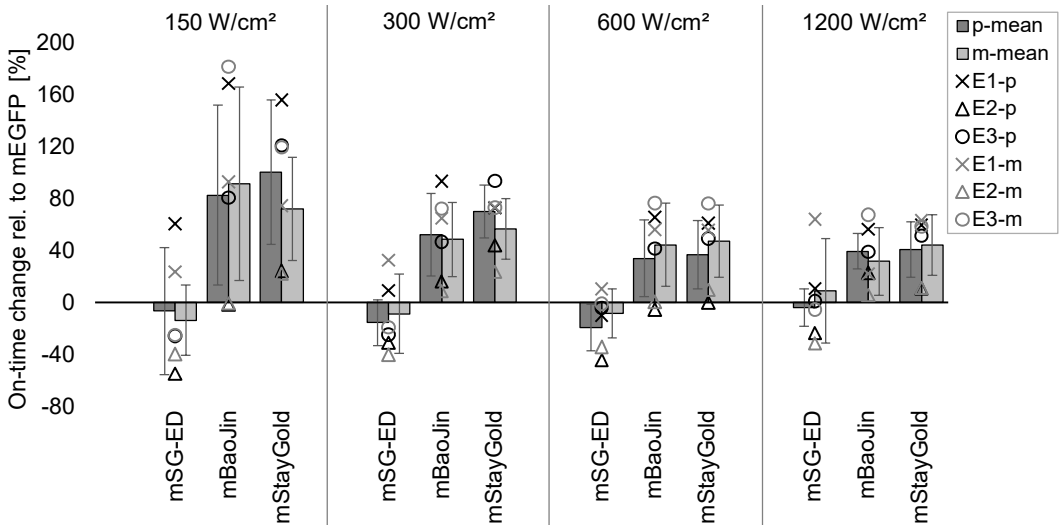

FIGURE 3.7: The change in on-time mean values (from Figure 3.6) of the mStayGold variants in relation to mEGFP. The symbols represent the change observed in each experiment (E1-E3), while the bars and their corresponding error bars show the combined mean change per setting and protein and the standard deviation of the experimental mean values, depending on the algorithm used (-p or -m).

Off-times

The off-times represent the durations during which a fluorescent protein remained in its non-fluorescent state. They are also measured and displayed in frames. Since the MATLAB-based approach directly results in the off-time information and it was

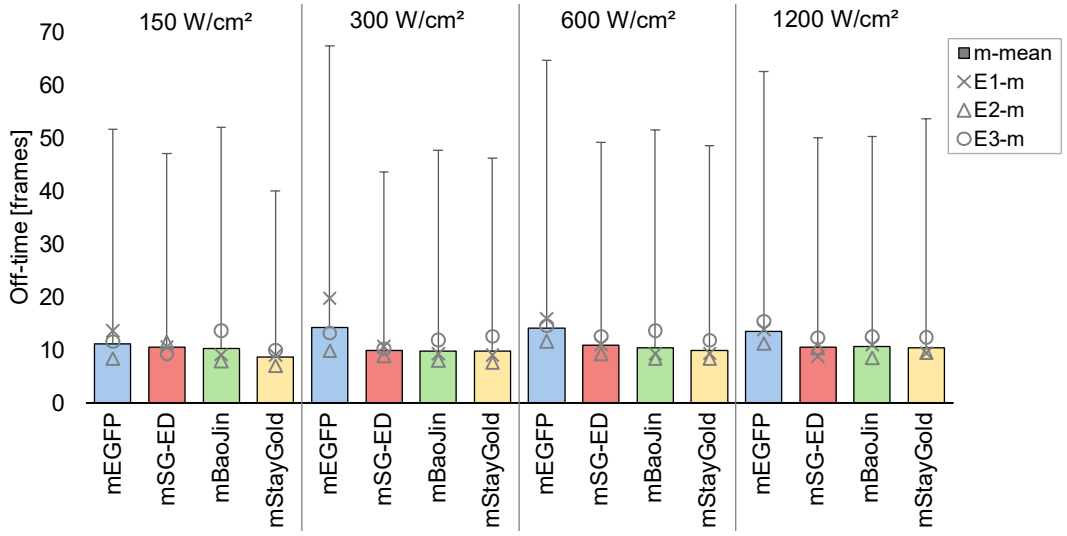

FIGURE 3.8: The resulting single-molecule off-times from all three experiments and their overall mean values for all laser intensities and illumination times were obtained on immobile lipid bilayers.

not achieved to retrieve that information from the *trackpy*-algorithm, only values from the first approach are presented. The resulting off-times mean values (Figure 3.8), were comparable across all laser intensities used, ranging between five and fifteen frames. From plotting the off-time histogram (not shown here), we observed a peak at short off-times followed by a rapid decay towards longer off-times. However, in all samples, a small subset of particles exhibited off-times exceeding 100 frames, corresponding to improbably long total off-times of 1 to 8 seconds during illumination, depending on the experimental settings. A possible explanation for this anomaly could be spikes in background signal noise being falsely registered as localizations. Although these instances were rare, their large values noticeably would increase the standard deviation and mean value. To address this, we treated these outliers as errors and excluded them from the subsequent analysis. The off-time change relative to mEGFP (Figure 3.9) demonstrated a clear change towards shorter off-times for all three mStayGold variants at laser intensities greater than 150 W/cm². The mStayGold variant also showed a clear decrease at 150 W/cm². The total mean decrease in off-times across all laser intensities for mSG-E138 resulted in -9.4% ± 8.8, for mBaoJin -14.8% ± 8.1 and for mStayGold -20.1% ± 6.3.

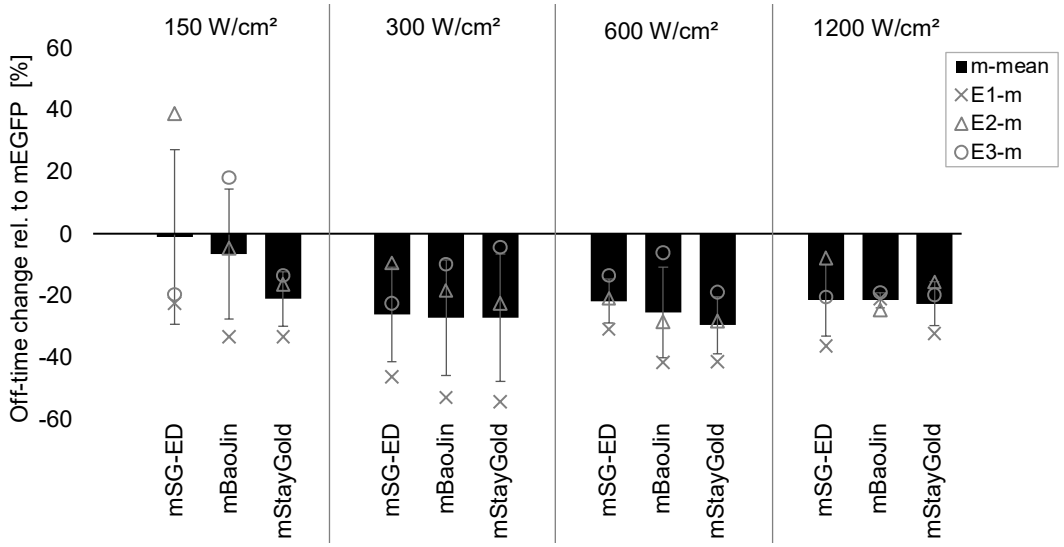

FIGURE 3.9: The change in off-time mean of the mStayGold variants (Figure 3.8) compared to mEGFP at the indicated intensity levels.

With the increase in on-times and a decrease in off-times for mStayGold variants, a higher fluorescent output was proven over a specific time frame. However, for determination of the lifetimes of the fluorescent proteins, it is essential to measure the number of localizations until photobleaching.

Number of localizations

The number of localizations refers to the total number of frames in which the particle was detected in its active state across the 300 frames total recording duration. The resulting number of mean number of localizations (Figure 3.10) ranged between 30 and 100 frames per experiment and showed a pronounced increase for mBaoJin and mStayGold compared to mEGFP across all settings. With higher excitation intensities and increasing photobleaching, the number of localizations decreased.

The total change relative to mEGFP (Figure 3.11) demonstrated a substantial increase in the number of localizations for both mBaoJin and mStayGold, reaching up

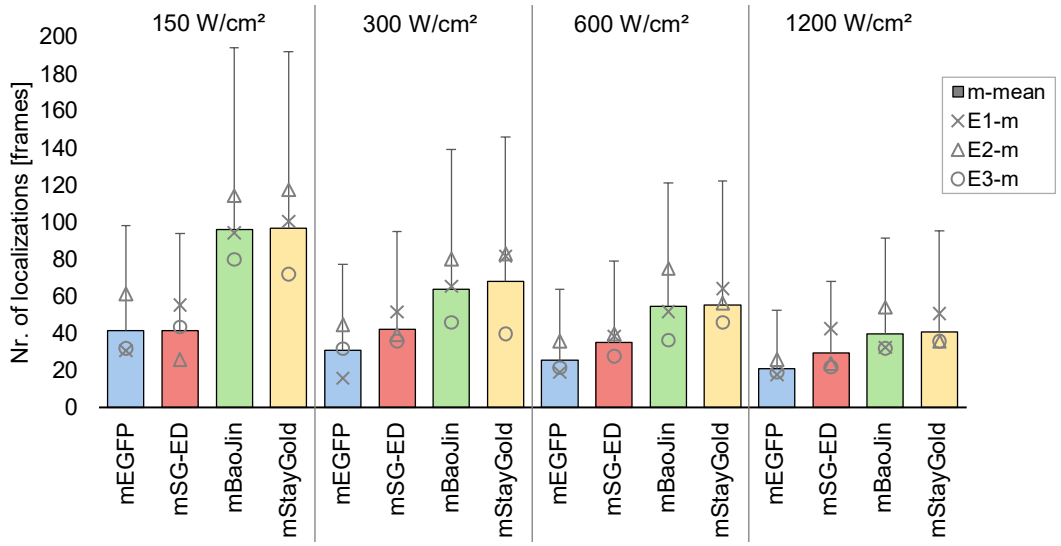

FIGURE 3.10: The resulting single-molecule localizations per fluorescent protein from all three experiments (E1-3) with the respective laser intensity settings on immobile lipid bilayers using the MATLAB approach.

to 400% in one experiment (mStayGold at 300 W/cm²). The strong increase was consistent for all laser intensities and experiments, yielding an average increase of +127.7% ± 56.2 for mBaoJin and +144.8% ± 91.9 for mStayGold. For mSG-E138D, a slight increase in the number of localizations was observed in some settings but was inconclusive for others, resulting in a total change of 48.0% ± 67.4.

The strong increase in the total number of localizations for mStayGold is highly beneficial for all fluorescence microscopy applications. The last single-molecule blinking parameter, the number of actual gaps reflecting the true number of blinks, is determined to further characterize fluorescent protein blinking behavior.

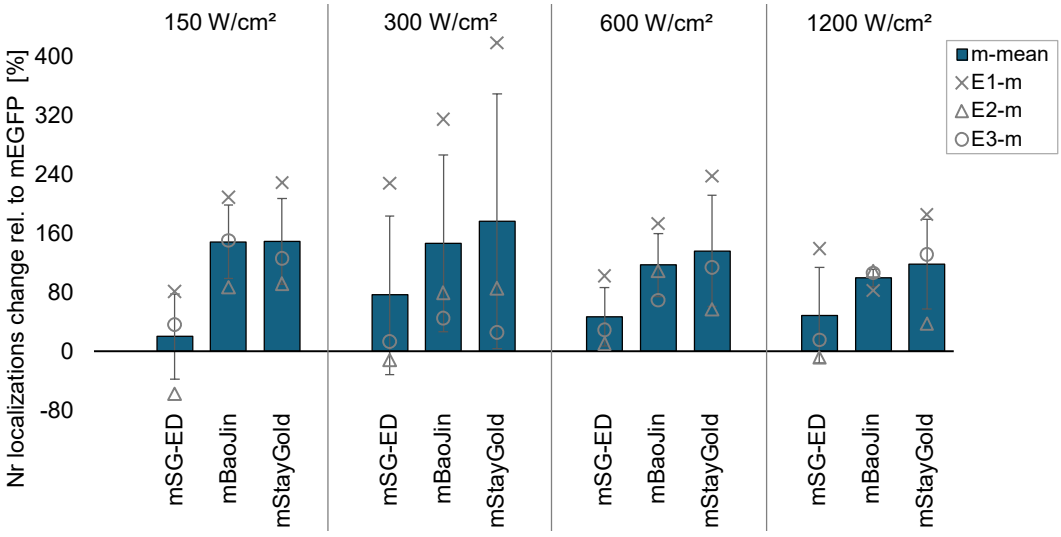

FIGURE 3.11: The change in the number of localizations per protein mean values of the mStayGold variants (Figure 3.10) compared to mEGFP at the indicated intensity levels.

Number of gaps

The number of gaps refers to the number of time spans the fluorescent protein was not detected and is quantified in absolute counts rather than in frames. The number of gaps is directly related to the number of blinks. The resulting total mean number of gaps per fluorescent protein (Figure 3.12) ranged from 8 to 15 with small deviations between variants. The values remained stable across all laser intensities with a small decay towards increased intensities.

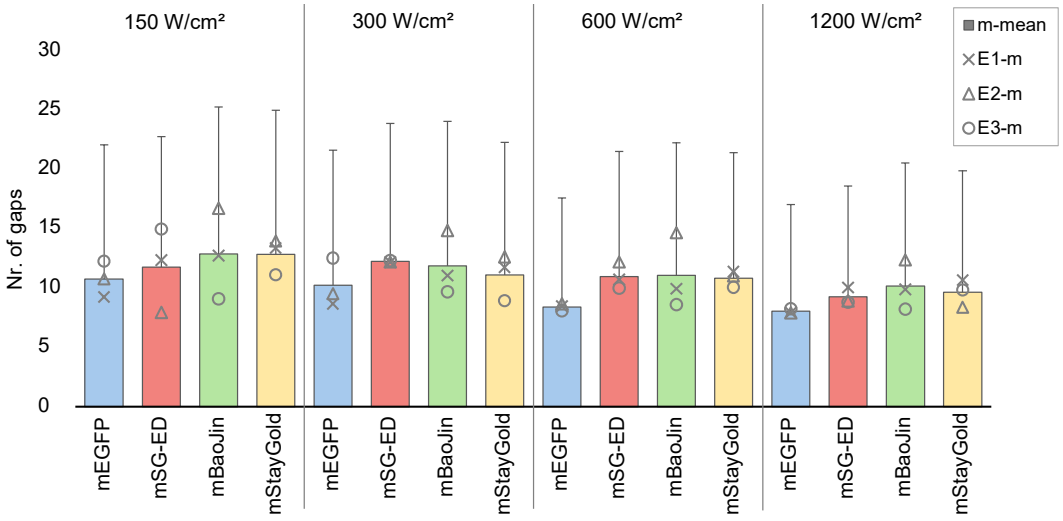

FIGURE 3.12: The resulting number of gaps per single-molecule fluorescent protein from all three experiments with the respective laser intensity settings on immobile lipid bilayers.

The total change of the mean number of gaps in respect to mEGFP (Figure 3.13) was not as strong as in the other blinking parameters, but still a small increase was detected for all experiments. The mean change across all experiments and laser intensity settings results in +19.5% ± 14.9 for mSG-E138D, +21.0% ± 24.1 for mBaoJin and +16.5% ± 22.4 for mStayGold.

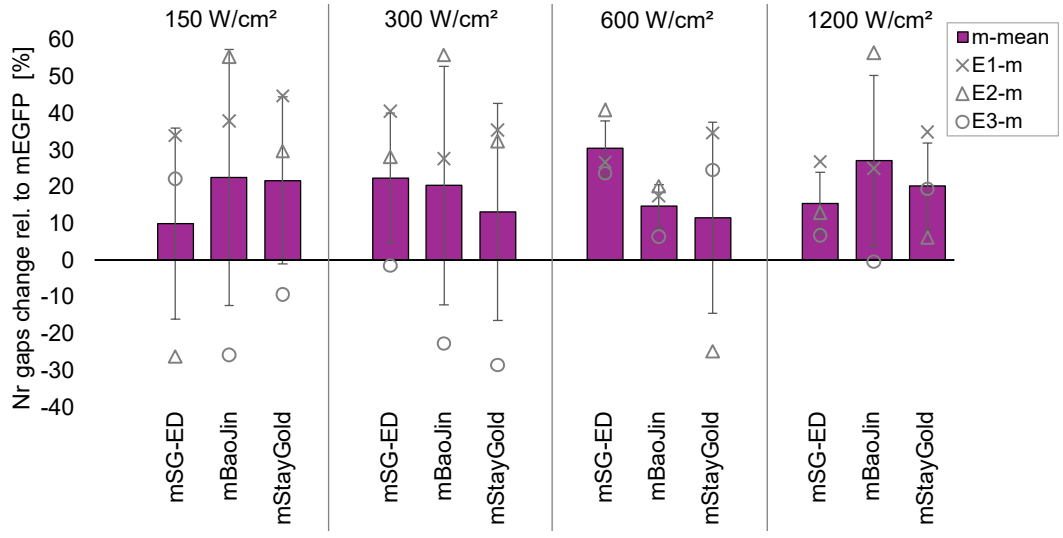

FIGURE 3.13: The change in the number of gaps per protein mean values of the mStayGold variants (Figure 3.12) compared to mEGFP at the indicated intensity levels.

Small increases in the number of gaps highlight that for mStayGold and mBaoJin, where the on-times are strongly enhanced, already a small increase in the number of blinks can lead to a substantial increase in total lifetime or total localizations, as observed earlier.

3.2.2 Single-molecule Brightness

The brightness values represent the integrated Gaussian-fitted intensity of the camera pixels within a defined area and were calculated to represent the absolute number of photons emitted per fluorescent protein. The resulting values (Figure 3.14) showed that mStayGold was brightest in all power settings measured. Also, it was shown that while the m-approach results in slightly lower brightness values, the difference between the algorithms was marginal and the tendencies between variants were comparable.

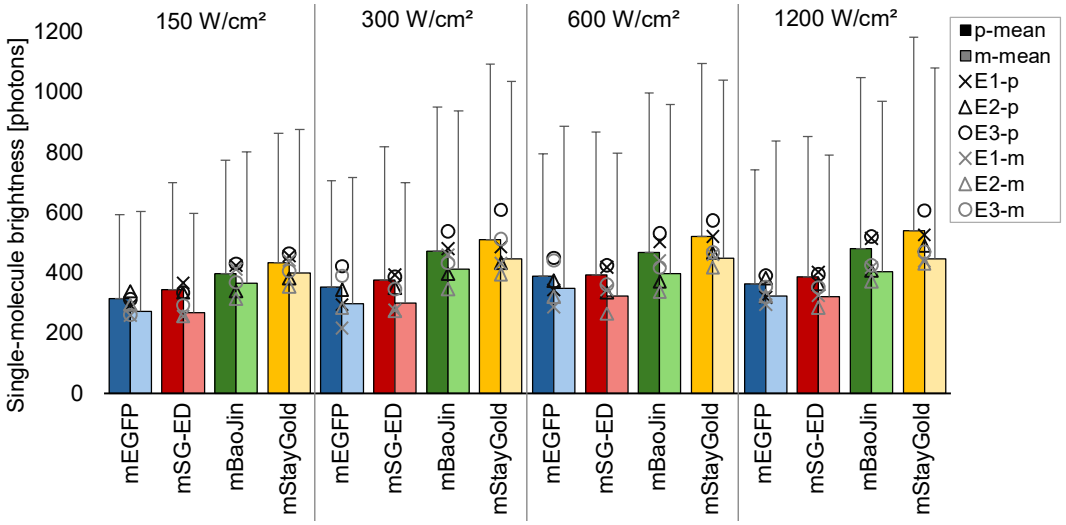

FIGURE 3.14: The resulting single-molecule brightness in photons per fluorescent protein from three experiments (E1-E3) and both algorithms (-p and -m) with the respective laser intensity settings (150 W/cm² + 80 ms, 300 W/cm² + 40 ms, 600 W/cm² + 20 ms and 1200 W/cm² + 10 ms) on immobile lipid bilayers. The bars represent the overall mean value of all experiments under each condition, along with the corresponding standard deviation.

With increasing laser intensities, the absolute brightness values increased. This effect was intended to be minimized through the adjustment of the illumination times. However, some residual influence appears to persist due to variations in algorithm detection efficiencies or fluctuations during the long illumination/recording times of up to 80 milliseconds. The single-molecule brightness changes in respect to mEGFP (Figure 3.15) revealed a strong increase for both mBaoJin and mStayGold across all experiments with increases up to 100% for one experiment at 300 W/cm² laser intensity. Notably, the mStayGold results exhibit a more pronounced change compared to mBaoJin across all experiments. The mStayGold changes yielded +42.2% ± 15.7 for the Python-based approach (-p) and +44.0% ± 20.3 for the MATLAB-based method (-m) and the mBaoJin changes were +29.5% ± 20.57 (-p) and +31.9% ± 26.2. The mSG-E138 variant results show a marginal increase in brightness for some experiments, however, a decreased brightness for others.

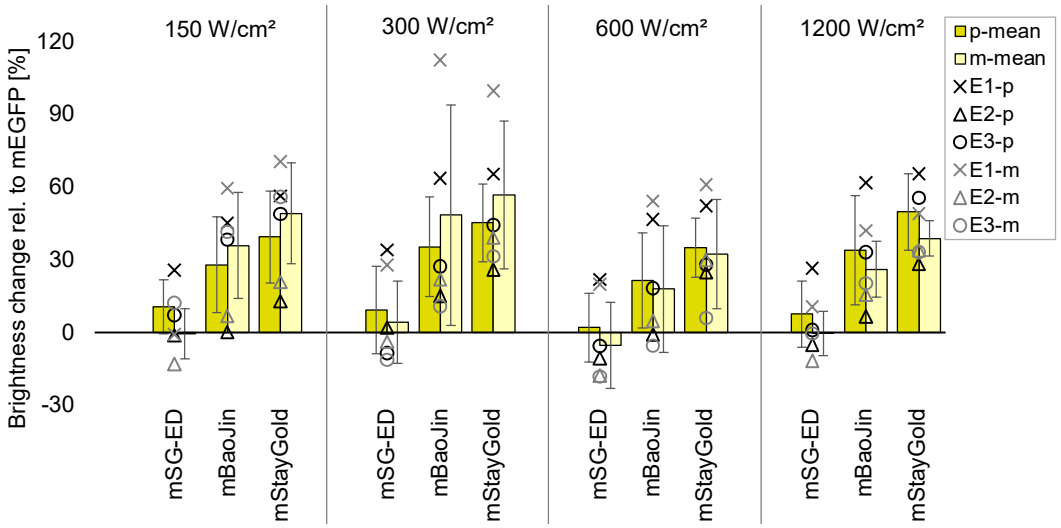

FIGURE 3.15: The change in single-molecule brightness mean values of the mStayGold variants (Figure 3.12) compared to mEGFP at the indicated intensity levels.

When assessing the absolute brightness of an object using a microscope, it is essential to consider the wavelength-dependent transmission of all optical components along the emission pathway. Therefore, a filter correction factor was established that uses the published emission spectra on *FPbase* [37] of the respective proteins and integrates the area over the wavelengths allowed to pass through the emission filter (Figure 3.16). This additional consideration of the wavelength-dependent transmission of the filter enables the determination of the percentage of fluorescence emission passing through the filter towards the camera for each protein. For mEGFP, 73% of the emitted fluorescence is transmitted, while mSG-E138D allows 77.9%, mBaoJin 77.4% and mStayGold 84.6% of their respective emission to pass.

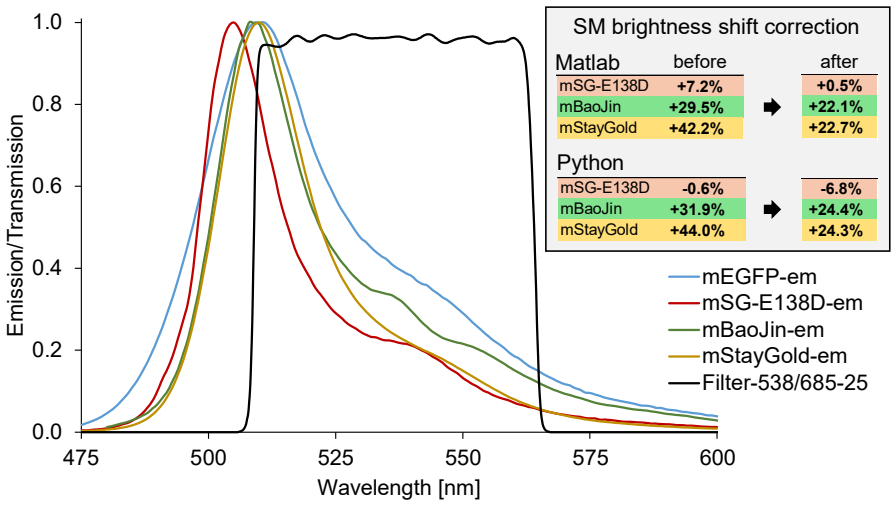

FIGURE 3.16: The illustration shows the wavelength-dependent emission spectra of the proteins used in this work and the transmission spectrum of the emission filter. The inlet table is showing the original mean single-molecule brightness change in respect to mEGFP (before) and the resulting corrected values after applying the filter correction for both localization approaches (after).

To account for these differences in the final results, a correction for each type of protein was performed by dividing the raw data mean value results by the respective fraction of the transmitted fluorescence through the filter. Subsequently, the resulting brightness changes relative to mEGFP were calculated again. Figure 3.16 includes a table exhibiting the corrected brightnesses in respect to mEGFP, depicting very similar corrected brightness changes of +22.1% (-p) and +24.4% (-m) for mBaoJin and +22.7% (-p) and +24.3% (-m) for mStayGold. Although the filter correction reduced the absolute brightness increases, they are clearly measurable. While the brightness change for mStayGold-E138D was already at zero, adding the filter correction resulted in a total decrease in brightness compared to mEGFP.

Discussion of the single-molecule results

In conclusion, the single-molecule blinking and brightness analysis showed strongly enhanced properties for mBaoJin and mStayGold. In general, these properties align with the findings projected in previous works from bulk cell experiments with low-intensity, continuous illumination as listed in Chapter 1, while some differences were established.
The general claim that mStayGold exhibits a photostability one magnitude higher than conventional fluorescent proteins [18][21] can be compared with the total number of localizations observed in this work. Here, while some experimental settings of mStayGold achieved increases of 400% (5-fold) in the number of localizations compared to mEGFP, across all experimental settings, the mean change results rather in a 2.5-fold increase. More specifically, Ando et al. [21] performed one experiment under 1000 W/cm² continuous wide-field illumination and resulted in a 5-fold change of mStayGold compared to mEGFP, while in the bilayer experiments here, the mean change of mStayGold in respect to mEGFP just doubled at 1200 W/cm². In contrast, live cell experiments by Zhang et al. [22] demonstrated the mStayGold photostability to be 1.5 to 3.5 times higher than mBaoJin, depending on the excitation intensity used (5.9 to 12 W/cm²), while this work did not find considerable differences in the number of localizations between mBaoJin and mStayGold. Viola et al. [26] compared the photostability of protein-tagged nanocages carrying 60 fluorescent proteins in live cell experiments, showing a 2.5-fold increase in mStayGold half-lifes compared to mEGFP. While this result is nicely comparable to the measured single-molecule number of detections results, they did not result in an increased photostability for mBaoJin compared to mEGFP. This finding does not align with the single-molecule results from this work, highlighting the variability of experimental contexts.
The brightness change derived by Ando et al. [21] using live cell experiments projected a three- to fivefold increase in brightness for their mStayGold variant (mStayGold). Zhang et al. [22], on the other hand, found that the intracellular brightness of mBaoJin and mStayGold was consistently higher than mEGFP by 70% to 140%. While the single-molecule brightness changes in respect to mEGFP in this work (+23% for mBaoJin and +24% for mStayGold) fall within the range reported by Zhang et al., they are considerably lower than the findings from Ando et al. Ivorra-Molla et al. [19] showed a comparison of the cellular brightness distribution for freely expressed mStayGold and mSG-E138D, resulting in large deviations across two orders of magnitude of individual measurements of each protein. Still, they did not result in differences between the two variants, contrary to the single-molecule results from this work, where mStayGold resulted in brighter single molecules than mSG-E138D.

The brightness and photostability in live cell experiments can be influenced by various factors such as transcription/translation rates, folding or maturation [19]. Also, the environment of the fluorescent proteins differs considerably between the experiments presented here. In the bilayer experiments the fluorescent proteins are exposed to the PBS buffer, whereas in live cell experiments, they are within an intracellular environment, completely different in terms of density, pH or affinity with surrounding molecules. Lastly, the experimental conditions, especially the excitation intensity, deviated considerably between the published results and those of this work. In total, a direct comparison of the values to the low-intensity live cell experiments is difficult while the overall statement was proven for the main results.

3.3 Bulk vs. single-molecules

In this section, an attempt is made to establish a direct comparison between single-molecule results and bulk results using the method outlined in Chapter 2.4.3. The photobleaching behavior of the bulk experiments and the single-molecule experiments from above over total illumination time was compared at three laser intensity settings (Figure 3.17). The photobleaching curves for both approaches showed comparable trends. An initial step can be observed in the calculated single-molecule curves as the initial value at t=0 is not registered in the accumulated density and the second value is the first depicted as a horizontal line.

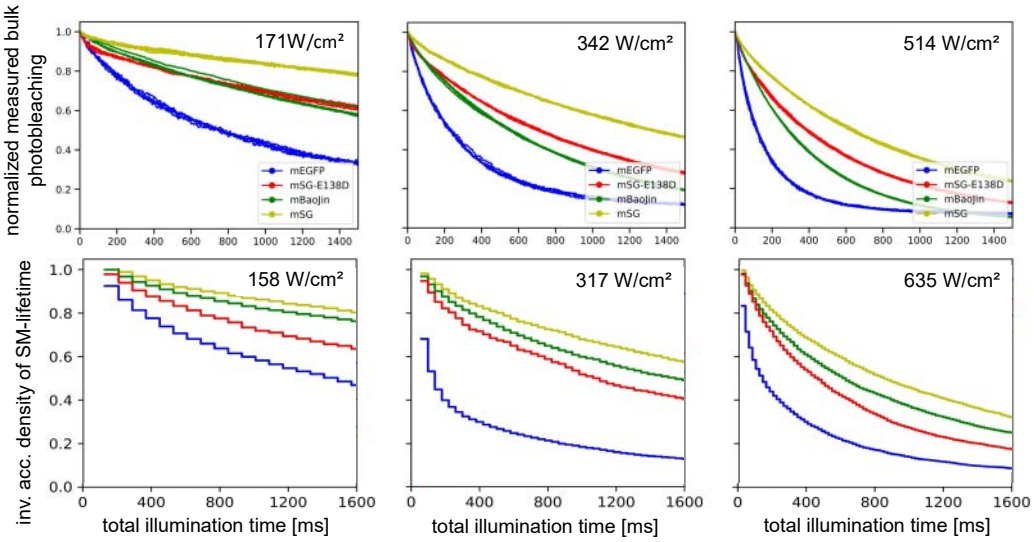

FIGURE 3.17: The normalized measured bulk photobleaching curves over total illumination time, including three laser intensities (top) and the curves for the inverted accumulated single-molecule density on-times (bottom). The bulk data points were retrieved from Chapter 3.1 and the single-molecule data originated from experiment one in Chapter 3.2.

Including all experiments performed in this work and using a more quantitative comparison, all results were fitted using the bi-exponential model approach and subsequent calculation of the half-life (Chapter 2.4.3). In the resulting plot (Figure 3.18) the calculated half-life for the SM- (light) and the bulk-experiments (dark) align well, indicating that the bulk experiment findings are directly supported by the single-molecule analysis. Consistent with the previous findings, increased half-life for mStayGold and mBaoJin compared to the other proteins were observed for both approaches, while mStayGold showed the longest half-life. The direct extraction of the half-life, defined as the point at which the brightness curves reach half of their

initial value, was also performed and resulted (Figure A.7) in similar observations of improved half-life for mBaoJin and mStayGold. Due to variability in the real measured laser intensities across all experiments, the results were collected matching the laser intensity best: Energy 1: 150 W/cm², Energy 2: 300 W/cm², Energy 3: 600 W/cm² and Energy 4: 1200 W/cm². The measured laser intensities are depicted in the respective chapters 3.1 and 3.2.

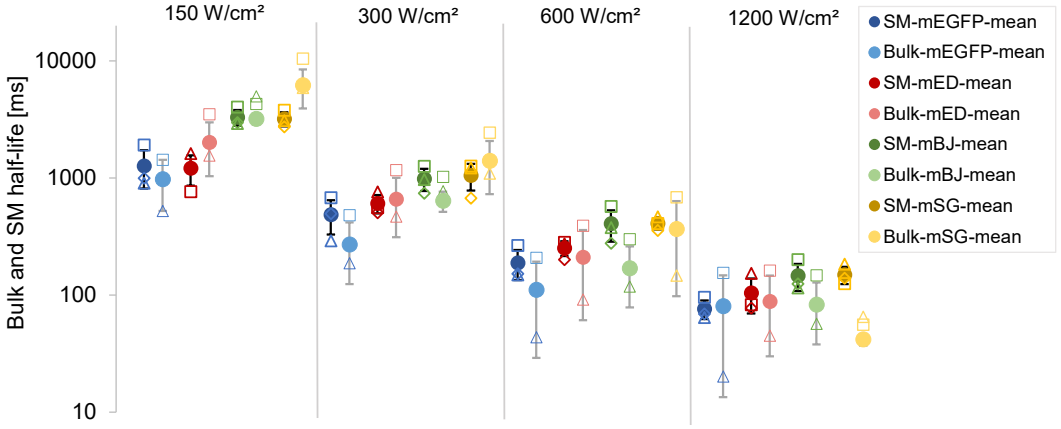

FIGURE 3.18: The logarithmic calculated half-life of bulk (dark) and single-molecule (bright) photobleaching curves, including two bulk experiments and three single-molecule experiments, where the individual experiments mean values are marked as square, cross and triangle, are presented. The total mean values (filled circles) and the respective standard deviations were derived for the respective method (bulk or SM).

Although the trends in single-molecule and bulk photobleaching half-lifes were comparable, calculating the absolute changes in single-molecule half-life compared to mEGFP yielded results in half-life increases of +152%, +116% and +117% for 150, 300 and 600 W/cm², respectively. These changes are significantly lower than those observed in bulk measurements under similar conditions, which showed half-life increases of +840%, +530% and +330% compared to mEGFP. Since the bulk half-lifes also were determined from normalized bleaching curves, changes between proteins in suface density or number of active fluorophores should not influence the results, this large difference can not be explained at this point. Similar discrepancies between single-molecule and bulk measurements were observed for both other fluorescent protein variants.

After extensive verification of the bulk and single-molecule characteristics of the protein variants, several additional factors needed to be addressed to ensure broad applicability of the findings.

3.4 Mobile vs. immobile proteins

Up to this point, the characterization was performed exclusively with immobile bilayers, as the movement of the fluorescent proteins complicates the tracking process. To confirm that the findings from above are applicable for mobile proteins, the same experiments were repeated using mobile bilayers. The single-molecule brightness values obtained from mobile bilayers and analyzed using the *DaoSTORM* + Python approach (Figure 3.19a) were comparable to those observed with immobile bilayers. The mobile results can be directly compared with the immobile results from Figure 3.14 using the *DaoSTORM* + Python approach. The trend of strongly increased

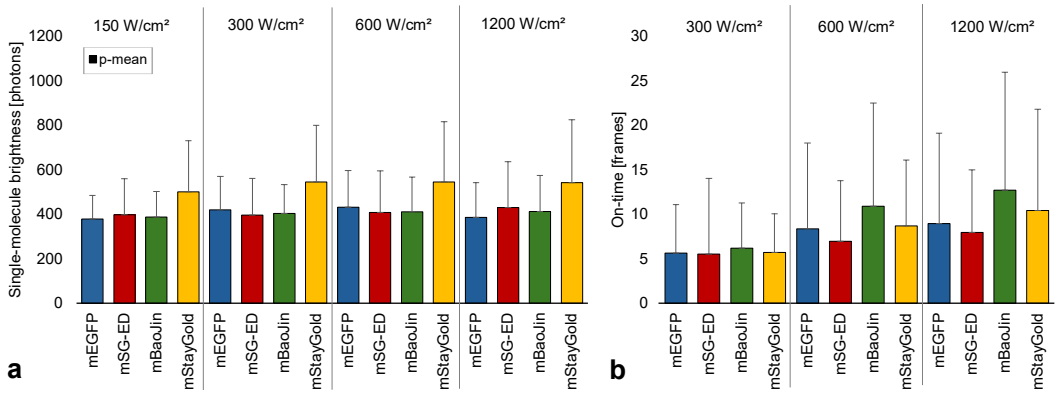

FIGURE 3.19: The single-molecule localization results on mobile bilayers, using the *DaoSTORM* + Python approach, are presented, displaying: **a**, the brightness in photons and **b**, the on-times of the fluorescent proteins from one experiment, including the respective excitation energies from the four excitation power steps (1200, 600, 300 and 150 W/cm²) with the increased illumination times (10, 20, 40 and 80 ms) as above. The analysis includes 19585 particles measured in 160 recordings total.

brightness for mStayGold compared to the other proteins was consistent with the immobile bilayer results. However, the increase in brightness for mBaoJin relative to mEGFP was less pronounced than in the immobile experiments. The on-time distributions (Figure 3.19b) displayed notable differences compared to those from immobile bilayers. Recording mobile signals with illumination times of 80 ms (at 300 W/cm²) resulted in substantial signal blurring, which made tracking difficult and yielded insufficient data for on-time analysis. For the remaining settings, the on-times also showed differences compared to the immobile results. First, an increase in on-times for higher laser intensities and shorter illumination times was determined. Secondly, the overall on-time values were lower than for the immobile bilayers (compare with Figure 3.6 -p). Among all settings, 1200 W/cm² laser intensity with 10 ms illumination time matched the immobile results most closely. Upon reviewing the raw tracking data from the experiments, it became evident that the reduced on-times were directly linked to the algorithm's decreased detection efficiency at longer illumination times and lower laser intensities. One potential post-measurement approach to address this issue would be to lower the detection threshold. However, this would significantly increase false positive detections due to background noise. These findings suggest that illumination times shorter than 20 milliseconds should be used to maintain sufficient tracking efficiency for mobile proteins with the algorithm applied here. Reviewing the on-time data for illumination times of 20 and 10 milliseconds, the mStayGold and mBaoJin variants still continued to exhibit increased on-times compared to mEGFP.

3.5 Varying excitation doses

Given the anticipated large differences in brightness and photostability among the proteins, the experimental setup was carefully designed to keep the excitation doses constant (laser intensity and illumination time) across all proteins. The use of high laser intensities and prolonged illumination times ensured that all proteins emitted a sufficient number of photons to achieve high signal-to-noise ratios, enabling accurate tracking and localization under all experimental conditions. However, to

ensure the broader applicability of these findings, alternative approaches and conditions were also investigated.

Selecting the 1200 W/cm² and 10 millisecond illumination setting as a reference, additional measurements were conducted at reduced imaging doses by decreasing the illumination time to 5, 2, and 1 milliseconds (Figure 3.20a). The resulting single-molecule brightness values as a function of the illumination times (Figure 3.20b) demonstrated a linear relationship for the mStayGold variants mean values, suggesting that the single-molecule brightness determination worked efficiently across the range of 1 to 10 milliseconds. On the other hand, the mean single molecule brightness of the mEGFP protein did not exhibit substantial increases over the range of 1 to 10 milliseconds illumination times, showing only a total brightness increase of 12.7% compared to 109.5% for mBaoJin or 178.3% for mStayGold. One possible explanation for this would be that the mEGFP proteins may begin photobleaching within the prolonged illumination times, though this seems unlikely given that Chapter 3.3 established the single-molecule half-life of mEGFP at 100 milliseconds, significantly longer than the maximum 10 milliseconds used here. For the mStayGold variants, where a linear increase was observed, a doubling of brightness over the range of illumination times would be expected. However, this was not observed, potentially due to localization algorithm errors during Gaussian fitting or nonlinearity from the camera chip resulting in errors in the raw data. Additionally, at illumination times below five milliseconds, the signal brightness was very low, possibly complicating localization as the signal differentiation from the background was difficult. While the specific causes of these phenomena remained unsolved in this study, the mStayGold variant consistently exhibited the highest brightness values across all measurements (Figure 3.20c). To minimize errors caused by localization

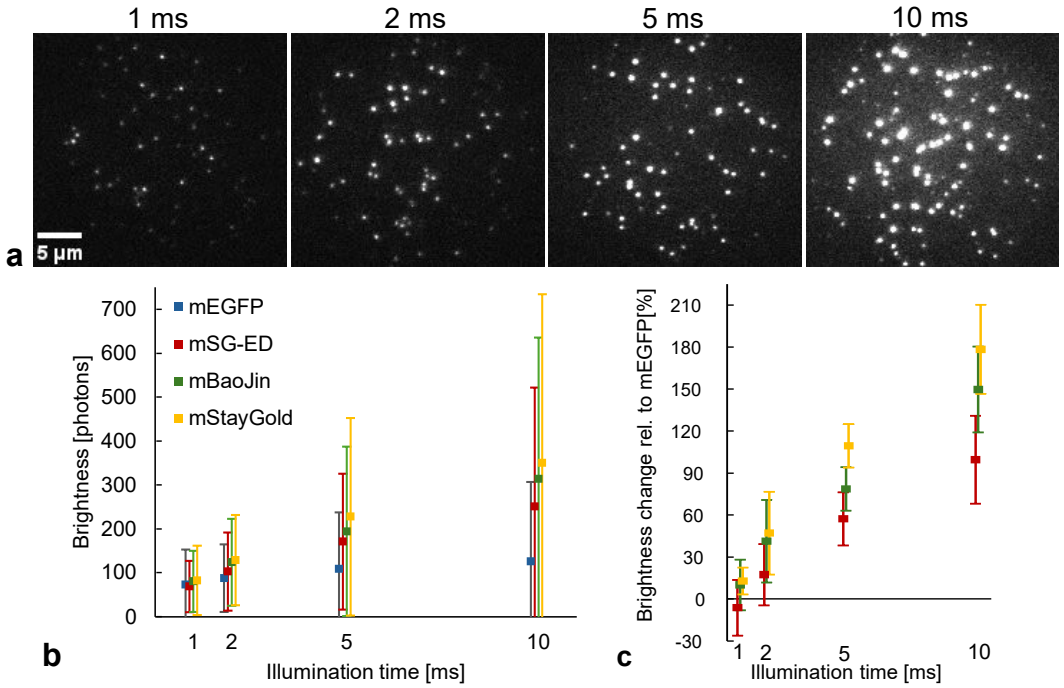

FIGURE 3.20: The results for the excitation dose-dependent recordings on immobile bilayers at 1200 W/cm², **a** under varying illumination times (1, 2, 5 and 10 ms), **b** the mean single-molecule brightness values in photons derived using the *ThunderSTORM* + MATLAB approach for the respective settings and **c** the changes in single-molecule brightness values compared to mEGFP.

algorithm inaccuracies, it is recommended to limit the illumination time to lower than 10 milliseconds and higher than 2 milliseconds. Despite these considerations on the effectiveness of the analysis, the conclusion of mStayGold being the brightest protein measured in these experiments remains valid.

Further investigation of potential saturation effects of the fluorescent proteins was conducted using 600 W/cm² for excitation and the same illumination time settings as for the 1200 W/cm² experiment (Figure A.8a). Under ideal conditions, the single-molecule brightness at 1200 W/cm² would be expected to be twice as high as compared to 600 W/cm² for equal illumination times, given a linear relationship between excitation dose and photon emission. The comparison of the 1200 W/cm² brightness compared to the 600 W/cm² brightness was performed for 10, 5 and 2 milliseconds illumination time. Comparing the difference between the two laser intensity settings in single-molecule brightness at equal illumination times resulted in +45.8% for mSG-ED, +44.8% for mBaoJin and +49.2% for mStayGold, total. Potential explanations for this discrepancy include saturation effects in the fluorescent proteins, which could limit their ability to emit photons proportionally to increased excitation intensity, or errors in the localization algorithm or sample preparation in the 600 W/cm² dataset. While the exact cause of this effect was not further investigated in this study, it is an important observation that requires close monitoring in future experiments.

As a last remark, the influence of varying excitation doses on the single-molecule blinking parameters was investigated. The single-molecule blinking parameters for all recordings from both intensity settings (1200 W/cm² and 600 W/cm²) and the respective illumination times were determined using the *ThunderSTORM* + MATLAB approach. The resulting mean value distributions (Figure A.8b) were used to calculate the relative change in respect to mEGFP. Summarizing the total changes across all settings, including both laser intensities and all illumination times (Table 3.1), revealed a strong increase in on-times and number of localizations for mStayGold and mBaoJin while the off-times decreased. These findings underline the results from the previous experiments, demonstrating that the superior performance of mStayGold and mBaoJin over mEGFP holds across a range of excitation conditions.

in [%]	On-times	Off-times	Nr of loc.	Nr of gaps
mSG-E13BD	-3.4 ±1.6	-11.3 ±2.9	+21.8 ±11.8	+20.7 ±10.5
mBaoJin	+42.1 ±8.7	-24.2 ±9.2	+84.7 ±15.1	+19.9 ±14.4
mStayGold	+53.7 ±6.4	-21.4 ±5.7	+96.0 ±35.1	+17.1 ±15.1

TABLE 3.1: The resulting total blinking parameter changes (in percent) relative to mEGFP combining all excitation energies and illumination time settings. The blinking parameters include the on-times, off-times, number of localizations and number of gaps.

Taking a closer look at the illumination time-dependent single-molecule blinking parameters, the changes from the initial settings of 10 milliseconds and 1200 W/cm² as well as 20 milliseconds and 600 W/cm² were plotted for direct visualization of the effect on each protein (Figure 3.21). As anticipated, shorter illumination times, which reduce photobleaching effects, led to an increase in the number of localizations and gaps. On the other hand, both the on-times and the off-times decreased by up to 40%, a notable but not extreme reduction. One possible explanation for these findings would be that lower excitation doses may result in undetected signals

of single molecules with low brightness due to limitations in the localization algorithm. During one single localization process of a particle over all frames, missing a true detection during one long on-time would contribute as two shorter on times and one short off-time in the statistics. This effect would account for both observed phenomena, shorter on-times and off-times and would additionally result in an increased number of gaps. However, the total number of localizations would only marginally decrease, as the loss of one detection contributes minimally to the overall statistics. It is highly likely that a combination of these effects is contributing to the observed behavior, highlighting a natural limitation of the localization algorithm with low illumination times.

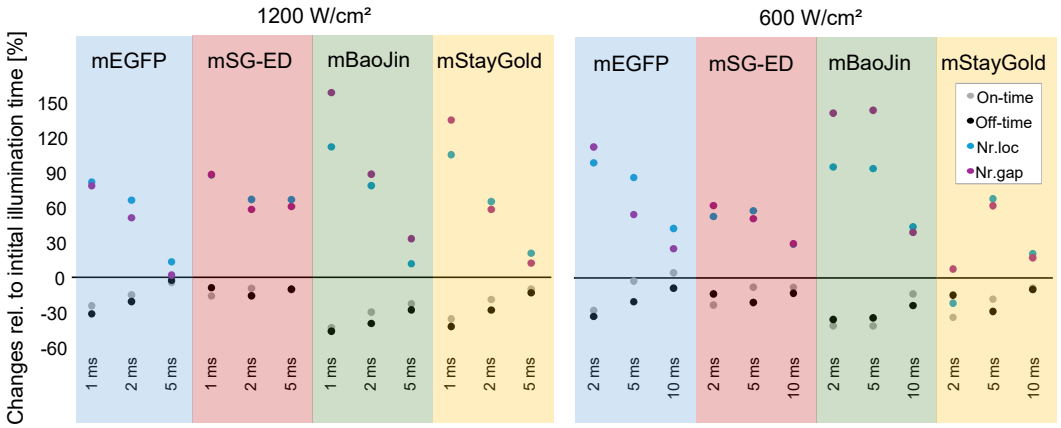

FIGURE 3.21: The resulting changes from the initial excitation dose settings (1200 W/cm² with 10 ms and 600 W/cm² with 20 ms) are summarized for each reduction step: 5 ms, 2 ms, and 1 ms for 1200 W/cm² (left) and 10 ms, 5 ms, and 2 ms for 600 W/cm² (right). The mean changes across these settings are illustrated for on-times (grey), off-times (black), number of localizations (blue), and number of gaps (violet). Each data point represents the mean value of 5 measurements and the total analysis adds up to 10607 particles localized in 160 recordings total.

3.6 Stroboscopic illumination

In addition to the evaluation of the improved single-molecule photostability and brightness of the newly developed mStayGold variants, an attempt was made to further reduce photobleaching of the fluorescent proteins by implementing the stroboscopic illumination strategy (see Introduction-Photobleaching). In this approach, the total illumination time of five milliseconds was maintained, but the continuous illumination was divided into 2,500 microsecond pulses, each lasting two microseconds, to ensure an equivalent total excitation dose. The interval between these microsecond pulses was varied between two and four microseconds to examine the impact of pause duration on photobleaching reduction.

Single-molecule blinking parameters

In total, two experiments were conducted on immobile lipid bilayers using laser intensities of 600 W/cm² and 1200 W/cm². The resulting blinking distributions for samples illuminated conventionally and those subjected to stroboscopic illumination (with either two or four microseconds pause time) were calculated using the

ThunderSTORM + MATLAB approach (Figure A.9). Comparing the blinking distributions of the different proteins, they consistently demonstrated that mStayGold exhibited the longest on-times, highest total number of localizations, shortest off-times, and largest number of gaps across both conventional and stroboscopic illumination. Still, the primary focus here was the change in blinking parameters resulting from the different illumination method. The changes in blinking parameters relative to conventionally illuminated recordings were calculated (Figure 3.22), revealing a modest increase in on-times for both mBaoJin and mStayGold across both experiments and delay times. The combined on-time changes across experiments and delay times resulted in +33.5% $\pm$ 34.4% for mBaoJin and 24.8% $\pm$ 12.1% for mStayGold. The off-time changes varied between experiments and resulted in a negligible total decrease of -6.6% $\pm$ 8.1% for mBaoJin and -5.0% $\pm$ 3.3% for mStayGold. The number of localizations showed a strong increase for mStayGold across both experiments and settings, resulting in 49.7% $\pm$ 6.1%. mBaoJin also exhibited a smaller but consistent increase of 16.8% $\pm$ 4.9%. However, the changes in number of gaps were inconclusive across all proteins and experimental conditions. For mStayGold-E138D, no increase in on-times was observed, while off-times and the number of detections increased slightly, by 9.7% $\pm$ 2.9% and 12.1% $\pm$ 13.4, respectively. mEGFP showed no measurable changes under the tested conditions. Additionally, it has to be noted that the mEGFP experiment using 600 W/cm² did not yield a functional bilayer, likely due to lipid bilayer formation issues, rendering it unmeasurable.

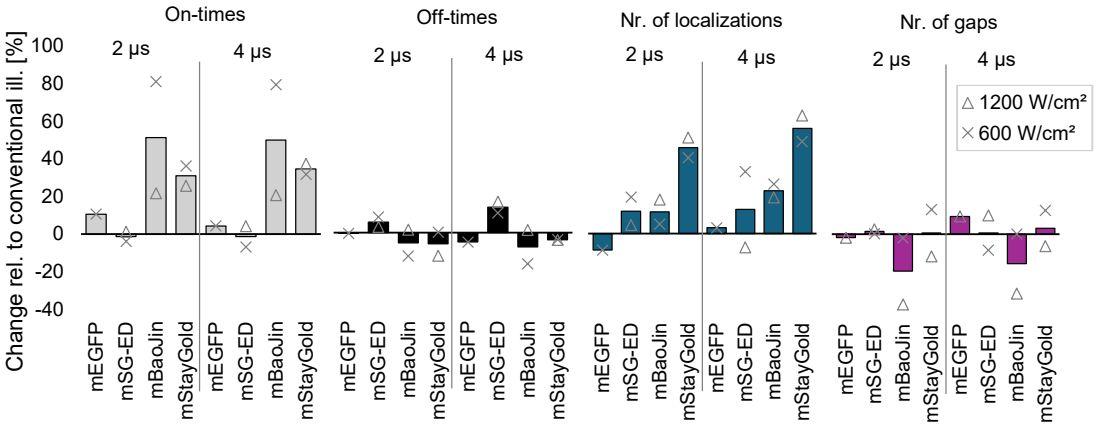

FIGURE 3.22: The mean changes in blinking parameters relative to conventional illumination for both stroboscopic settings of 2 µs and 4 µs pauses across two individual experiments, conducted at either 600 W/cm² (cross) or 1200 W/cm² (traingle). The mean value of five recordings per experiment and protein is depicted for the on-times, off-times, number of detections, and number of gaps as well as the combined mean value including both experiments. Each recording utilized a total illumination time of 5 ms per image, with measured peak laser intensities of 684 W/cm² and 1357 W/cm². A total of 17251 particles were analyzed across 150 recordings.

Single-molecule brightness

The results from the single-molecule brightness analysis (Figure 3.23 left) indicated a decrease in brightness for both stroboscopic settings in both experiments. Specifically, the brightness change under stroboscopic illumination (Figure 3.23 right) revealed a strong decrease for the experiment conducted under 1200 W/cm² laser intensity, while the experiment with 600 W/cm² showed only a modest reduction. Nevertheless, combining all measurements, the overall brightness decrease due to

stroboscopic illumination was calculated as -24.3% ±13.2% for mStayGold or -20.8% ±12% for mBaoJin. One potential source of error is the extended recording time compared to convantional illumination, which results from the 2500 on-off laser cycles. This extended duration could introduce time-dependent brightness fluctuations and movement artifacts. Such artifacts, caused by signal smearing during prolonged illumination, would be particularly relevant in experiments with mobile fluorescent proteins, where their impact could be more pronounced. However, for the immobile proteins measured in these experiments, this effect is expected to be minimal. Another possible factor is the pulse switching slew rate. According to Oxxius, the maximum analog modulation frequency for the L6Cc laser box is 1 MHz (1 µs). Given that the pulse lengths used in these experiments were 2 µs, they should remain within the laser's operational limits. Nevertheless, the interplay between all components involved in laser signal generation could affect the waveform edges and maximum value at high speed applications. For a more detailed investigation, monitoring these factors more closely is recommended.

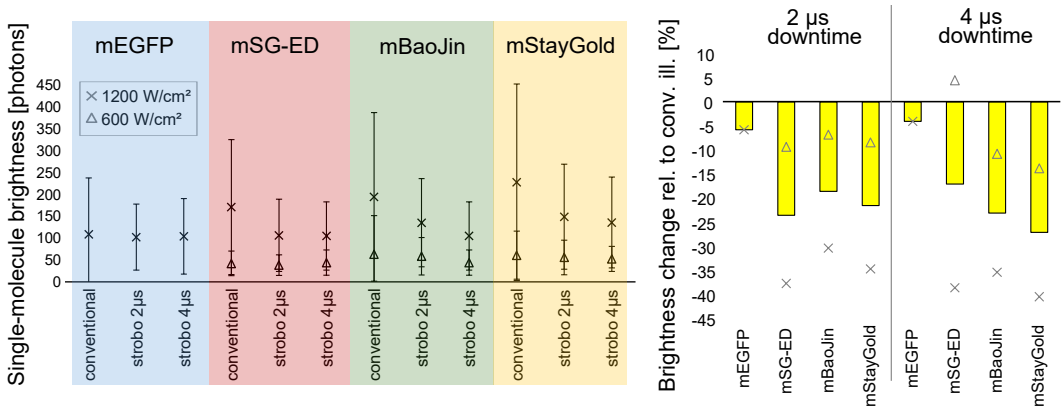

FIGURE 3.23: The single-molecule brightness in photons for 1200 W/cm² (cross) and 600 W/cm² (triangle) displayed across all three illumination settings (left) and the respective changes in mean single-molecule brightness relative to the conventionally illuminated recordings, are shown on the right. The bars represent the mean values of the changes.

For further clarity of the photobleaching depending on the illumination method used, the single-molecule photobleaching curves were determined from the number of detections distributions as performed in previous experiments. This approach allowed for the calculation of the single-molecule half-lifes depending on the method of illumination used across all experiments performed here (Figure 3.24).

The resulting half-life values were determined from bi-exponential fits to the decay curves and the mean changes relative to the conventionally illuminated recordings were calculated. The results showed that mEGFP and mSG-E138 did not exhibit measurable changes in photobleaching times with stroboscopic illumination. However, both mBaoJin and mStayGold demonstrated positive changes in half-lifes under stroboscopic illumination for both experiments and both off-time intervals used (Table 3.2). Additionally, a slight increase in half-life was observed when extending the pause duration from two to four microseconds, indicating a potential benefit of longer pause durations for these fluorescent proteins.

According to the literature [14], stroboscopic off-times exceeding one microsecond are considered optimal for ground state relaxation in fluorescent proteins. While an increase in half-life with extended pause times beyond one microsecond has not been documented before, the current findings may suggest additional influences

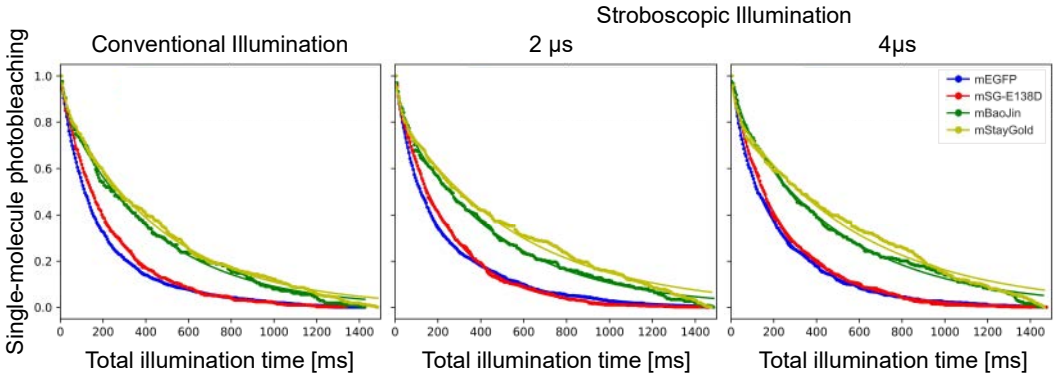

FIGURE 3.24: The single-molecule photobleaching curves were calculated from the number of localizations from the 600 W/cm² experiment, including the conventional illumination (left) and stroboscopic illumination of 2 µs pulses and either 2 µs pause (center) or 4 µs pause (right) between pulses. The bi-exponential fits for each protein were calculated using the combined nrumber of localizations distribution of five recordings per protein and setting and are shown as a solid line in the respective color.

Laser intensity	600 W/cm²		1200 W/cm²	
Pause time	2 µs	4 µs	2 µs	4 µs
mBaoJin	+10.2%	+30.4%	+21.0%	+22.2%
mStayGold	+31.2%	+42.8%	+64.0%	+75.8%

TABLE 3.2: The percentage changes in the calculated single-molecule photobleaching half-lifes in respect to the conventional illumination results for both experiments with either 600 W/cm² and 1200 W/cm² and across both delay times of 2 µs and 4 µs.

of photobleaching state dynamics or may simply reflect an additional effect resulting from the increased recording time per image. Nevertheless, a net increase in single-molecule half-lifes for mBaoJin and mStayGold in all experiments performed is given when using stroboscopic illumination.

Chapter 4

Conclusion

This thesis presents a comprehensive study of the single-molecule photobleaching and brightness properties of fluorescent protein variants of mStayGold, including mStayGold-E138D, mBaoJin and mStayGold, and compares them to conventional mEGFP. The fluorescent proteins were measured using supported lipid bilayers, facilitating either mobile or immobile fluorescent proteins. For the localization of single molecules, two distinct approaches were employed, *ThunderSTORM* and *DaoSTORM* while the tracking of the single molecules over time was performed by a custom-made MATLAB script or a Python-based analysis, respectively. Both approaches were rigorously evaluated to ensure the accuracy and reliability of single-molecule tracking. The resulting single-molecule data provided a full picture of the brightness and photobleaching characteristics, including parameters of the on-time, off-time, number of localizations and number of gaps (number of blinks). A variety of experimental parameters were controlled to ensure a valid statement on the performance of the mStayGold variants. The variations included, ranging the laser intensity from 150, 300, 600 and 1200 W/cm² while adjusting the illumination times (80, 40, 20 and 10 milliseconds) to ensure comparable excitation doses per recording. Additionally, the study explored the potential for further improving the photostability by using stroboscopic illumination. Therefore, the continuous illumination of five milliseconds per image was divided into 2500 bursts of two microseconds with two (or four) microseconds pauses.

The proteins were prepared on immobile lipid bilayers and for the mStayGold and mBaoJin proteins, the mean change compared to mEGFP resulting from the single-molecule blinking parameters demonstrated increased on-times of +56% for mStayGold and +53% for mBaoJin (Figure 3.7) while the off-times decreased by -25% for mStayGold and -20% for mBaoJin (Figure 3.9) across all experiments performed and all laser intensities used. The total number of detections also notably increased for both variants, resulting in +145% for mStayGold and +128% for mBaoJin (Figure 3.11). The total mean increase in number of blinks was not as pronounced, ranging below 20% (Figure 3.13). Nevertheless, this finding is in line with the previous results, as with a strongly increased on-time, a small increase of blinks already results in a strongly enhanced photon output per protein. In nearly all experiments and settings used, mStayGold outperformed mBaoJin, showing more stable and consistent improvements. The mSG-E138D variant, however, exhibited no substantial increase in on-times, a small reduction in off-times and only slight improvements in the number of localizations and the number of gaps compared to mEGFP. These results suggest a slightly increased performance of mSG-E138D compared to mEGFP that is far inferior to the other two variants.
The single-molecule brightness was determined for all fluorescent proteins (Figure 3.14) and corrected for the wavelength-dependent transmittance in the emission

path of the experimental setup according to the emission spectra of the fluorescent proteins (Figure 3.16). The resulting mean brightness changes compared to mEGFP showed a notable increase of +23% for mBaoJin and +24% for mStayGold across all settings (Figure 3.15). The mSG-E138D variant showed no increase in single-molecule brightness compared to mEGFP.
Additionally, single-molecule photobleaching curves were determined based on the number of localizations distribution in respect to the illumination time (Figure 3.17). A quantitative model was employed using a bi-exponential decay fitting of the bleaching curves for calculation of photobleaching half-lifes of both bulk and single-molecule photobleaching (Chapter 2.4.3). The results demonstrated that the bulk photobleaching results are directly correlated to the single-molecule results (Figure 3.18). Further, the results confirmed the significantly increased photostability for mBaoJin and mStayGold in both single molecules and bulk experiments.

While the results from above were determined using immobile lipid bilayers for simplifying the localization and tracking process with stationary signals, a further experiment was conducted using mobile lipid bilayers for validating the findings for mobile proteins. While the single-molecule brightness remained comparable for both approaches, tracking labels with lower photon outputs at lower laser intensities is much more challenging and the algorithms were less efficient under these conditions (Figure 3.19). Decreased tracking efficiency can lead to an overestimation of the number of gaps in combination with lower on-times and increased off-times.
Further, the impact of varying excitation doses on the proteins and the localization algorithms was tested. The illumination time per image was systematically reduced for two laser intensity settings (1200 W/cm² and 600 W/cm²) and the single-molecule blinking and brightness parameters were determined. First, testing the single-molecule brightness across decreasing illumination times revealed that illumination times below two milliseconds did not produce trackable signals (Figure 3.20). The changes in single-molecule blinking parameters also supported this observation, showing reduced on-times and off-times for shorter illumination times, likely due to signal loss during tracking (Figure 3.21). Second, a direct comparison of doubling the laser intensity at equal illumination times demonstrated brightness increases of approximately 50% for all mStayGold variants, suggesting potential saturation effects or other nonlinearities during data acquisition or analysis. Nevertheless, across all intensities and illumination times examined, the mStayGold and mBaoJin variant consistently showed strongly improved single-molecule blinking and brightness characteristics compared to mEGFP (Table 3.1).

The single-molecule results from experiments using the stroboscopic illumination approach showed improvement in photostability for mBaoJin and mStayGold. Compared to conventional illumination, the on-times increased by +25% for mStayGold and +33% for mBaoJin, while the total number of localizations increased by +50% for mStayGold and +17% for mBaoJin (Figure 3.22). However, there was no considerable change for mEGFP and mSG-ED measurable. Also, the off-times or number of gaps did not change considerably. A clearly enhanced photostability was demonstrated using the single-molecule photobleaching-curve method, resulting in increased half-lifes of up to 70% (Figure 3.24). Despite the improved photostability for both mBaoJin and mStayGold, the single-molecule brightness decreased under stroboscopic illumination across all conditions by -24% for mStayGold and -20% for mBaoJin (Figure 3.23). This decrease is likely a direct result of the elongated recoding times by the introduction of pause times. Although the photostability was

improved for mBaoJin and mStayGold, the reduced brightness and the extended recording time per image limit the utility of the stroboscopic illumination approach to certain types of applications.

The mStayGold variant, combining increased single-molecule on-time, reduced off-time and increased number of localizations in combination with increased single-molecule brightness compared to conventional mEGFP, does not only improve the tracking ability but also increases the effective photon yield, making mStayGold exceptionally well-suited for fluorescence microscopy approaches.

Bibliography

[1] D. Axelrod. Cell-substrate contacts illuminated by total internal reflection fluorescence. *J. Cell Biol.*, 89 (1):141–145, 1981.

[2] D. Axelrod. *Total Internal Reflection Fluorescence (TIRF) and Evanescence Microscopies*. 2053-2563. IOP Publishing, 2022.

[3] S. W. Hell and J. Wichmann. Breaking the diffraction resolution limit by stimulated emission: stimulated-emission-depletion fluorescence microscopy. *Opt. Lett.*, 19:780–782, 1994.

[4] M. Rust, M. Bates, and X. Zhuang. Sub-diffraction-limit imaging by stochastic optical reconstruction microscopy (STORM). *Nat. Methods*, 3:793–796, 2006.

[5] E. Betzing, G. H. Patterson, and R. Sourgrat et al. Imaging Intracellular Fluorescent Proteins at Nanometer Resolution. *Science*, 313:1642–4645, 2006.

[6] M. Moertelmaier, M. Brameshuber, M. Linimeier, G. J. Schütz, and H. Stockinger;. Thinning out clusters while conserving stoichiometry of labeling. *Appl. Phys. Lett.*, 87:263903, 2005.

[7] M. Brameshuber, F. Kellner, and B. K. Rossboth et al. Thinning out clusters while conserving stoichiometry of labeling. *Nat. Immunol.*, 19:487–496, 2018.

[8] C. Bodner and M. Brameshuber. *Determination of Biomolecular Oligomerization in the Live Cell Plasma Membrane via Single-Molecule Brightness and Co-localization Analysis*, pages 277–303. Springer International Publishing, 2023.

[9] O. Shimomura, F. H. Johnson, and Yo Saiga. Extraction, Purification and Properties of Aequorin, a Bioluminescent Protein from the Luminous Hydromedusan, Aequorea. *J. Cell. Comp. Physiol.*, 59:223–239, 1962.

[10] D. C. Prasher, V. K. Eckenrode, and W. W. Ward et al. Primary structure of the Aequorea victoria green-fluorescent protein. *Gene*, 111:229–233, 1992.

[11] C. Ringemann, A. Schönle, and A. Giske et al. Enhancing Fluorescence Brightness: Effect of Reverse Intersystem Crossing Studied by Fluorescence Fluctuation Spectroscopy. *Chem. Phys. Chem.*, 9:612–624, 2008.

[12] T. Cordes, A. Maiser, and C. Steinhauer et al. Mechanisms and advancement of antifading agents for fluorescence microscopy and single-molecule spectroscopy. *Phys. Chem. Chem. Phys.*, 13:6699–6709, 2011.

[13] G. Donnert, C. Eggeling, and S. W. Hell. Major signal increase in fluorescence microscopy through dark-state relaxation. *Nat. Methods*, 4:84–86, 2007.

[14] A.K. De and D.A. Goswami. A Systematic Study on Fluorescence Enhancement under Single-photon Pulsed Illumination. *J. Flouresc.*, 19:931–937, 2009.

[15] C. Boudreau, T.L. Wee, and Y.R. Duh et al. Excitation Light Dose Engineering to Reduce Photo-bleaching and Photo-toxicity. *Sci. Rep.*, 6:30892, 2016.

[16] L. Ludvikova, E. Simon, and M. Deygas et al. Near-infrared co-illumination of fluorescent proteins reduces photobleaching and phototoxicity. *Nat. Biotechnol.*, 42:872–876, 2024.

[17] M. Byrdin, C. Duan, D. Burgeois, and K. Brettel. A Long-Lived Triplet State Is the Entrance Gateway to Oxidative Photochemistry in Green Fluorescent Proteins. *J. Am. Chem. Soc.*, 140:2897–2905, 2018.

[18] M. Hirano, R. Ando, and S. Shimozono et al. A highly photostable and bright green fluorescent protein. *Nat. Biotechnol.*, 40:1132–1142, 2022.

[19] E. Ivorra-Molla, D. Akhuli, and M.B.L. McAndrew et al. A monomeric StayGold fluorescent protein. *Nat. Biotechnol.*, 42:1368–1371, 2024.

[20] J. Goedhart and T. W. J. Gadella. Breaking up the StayGold dimer yields three photostable monomers. *Nat. Methods*, 21:228–229, 2024.

[21] R. Ando, S. Shimozono, and H. Ago et al. StayGold variants for molecular fusion and membrane-targeting applications. *Nat. Methods*, 21:648–656, 2024.

[22] H. Zhang, G.D. Lesnov, and O.M. Subach et al. Bright and stable monomeric green fluorescent protein derived from StayGold. *Nat. Methods*, 21:657–665, 2024.

[23] S. Shimozono, R. Ando, and M. Sugiyama et al. Preprint: Comparison of monomeric variants of StayGold. *bioRxiv*, 2024.

[24] D. A. Zacharias, J. D. Violin, and A. C. Newton et al. Partitioning of Lipid-Modified Monomeric GFPs into Membrane Microdomains of Live Cells. *Cells. Science*, 296:913–916, 2002.

[25] M. Hirano, Y. Yonemaru, and S. Shimozono et al. StayGold photostability under different illumination modes. *Sci. Rep.*, 14:5541, 2024.

[26] G. Viola, K. A. Jacobs, and J. Lemière et al. Preprint: Quantitative comparison of monomeric staygold variants using protein nanocages in living cells. *bioRxiv*, 2024.

[27] M. Eeman and M. Deleu. From biological membranes to biomimetic model membranes. *Biotech., Agr., Soc. et Env.*, 14:719–736, 2010.

[28] J. A. Nye and J. T. Groves. Kinetic control of histidine-tagged protein surface density on supported lipid bilayers. *Langmuir*, 24(8):4145–4149, 2008.

[29] E. Hochuli, W. Bannwarth, and H. Döbeli et al. Genetic approach to facilitate purification of recombinant proteins with a novel metal chelate adsorbent. *Nature Biotechnology*, 6(11):1321–1325, 1988.

[30] J. Huppa, M. Axmann, and M. Mörtelmaier et al. TCR–peptide–MHC interactions in situ show accelerated kinetics and increased affinity. *Naure*, 463:963–967, 2010.

[31] R. Platzer, B. K. Rossboth, and M. C. Schneider et al. Unscrambling fluorophore blinking for comprehensive cluster detection via photoactivated localization microscopy. *Nat. Commun.*, 11:4993, 2020.

[32] T. Kuhn, J. Hettich, and R. Davtyan et al. Single molecule tracking and analysis framework including theory-predicted parameter settings. *Sci. Rep.*, 11:9465.

[33] L. Schrangl. sdt-python: Python library for fluorescence microscopy data analysis (19.0.1). Zenodo, 2024.

[34] H. Babcock, Y. M. Sigal, and X. Zhuang. A high-density 3D localization algorithm for stochastic optical reconstruction microscopy. *Opt. Nano.*, 1:6, 2012.

[35] D. B. Allan, T. Caswell, N. C. Keim, C. M. van der Wel, and R. W. Verweij. soft-matter/trackpy: v0.6.4 (v0.6.4). Zenodo, 2024.

[36] M. Ovesný, P. Křížek, J. Borkovec, Z. Švindrych, and G. M. Hagen. ThunderSTORM: a comprehensive ImageJ plugin for PALM and STORM data analysis and super-resolution imaging. *Bioinformatics*, 30:2389–2390, 2014.

[37] TJ. Lambert. FPbase: a community-editable fluorescent protein database. *Nat. Meth.*, 16:277–278, 2019.

Appendix A

Additional information

The following sequences refer to the fluorescent proteins used in this work that were produced by M.Sc. Lucia Cikatricisová under the supervision of Prof. Ario de Marco from the University of Nova Gorica.

Genetic sequence of mStayGold

MKHHHHHHVSTGEELFTGVVPFKFQLKGTINGKSFTVEGEGEGNSHEGSHKGKYVC
TSGKLPMSWAALGTSFGYGMKYYTKYPSGLKNWFHEVMPEGFTYDRHIQYKGDGSI
HAKHQHFMKNGTYHNIVEFTGQDFKENSPVLTGDMDVSLPNEVQHIPIDDGVECTV
TLQYPLLSDESKCVEAYQNTIIKPLHNQPAPDVPFHWIRKQYTQSKDDTEERDHIIQSE
TLEAHL*

Genetic sequence of mStayGold-E138D

MKHHHHHHASTPFKFQLKGTINGKSFTVEGEGEGNSHEGSHKGKYVC
TSGKLPMSWAALGTSFGYGMKYYTKYPSGLKNWFHEVMPEGFTYDRHIQYKGDGSI
HAKHQHFMKNGTYHNIVEFTGQDFKENSPVLTGDMNVSLPNDVQHIPRDDGVECPV
TLLYPLLSDKSKCVEAHQNTICKPLHNQPAPDVPYHWIRKQYTQSKDDTEERDHICQSE
TLEAHL*

Genetic sequence of mBaoJin

MKHHHHHHVSKGEEENMASTPFKFQLKGTINGKSFTVEGEGEGNSHEGSHKGKYVC
TSGKLPMSWAALGTTFGYGMKYYTKYPSGLKNWFREVMPGGFTYDRHIQYKGDGSI
HAKHQHFMKNGTYHNIVEFTGQDFKENSPVLTGDMNVSLPNEVPQIPRDDGVECPV
TLLYPLLSDKSKYVEAHQYTICKPLHNQPAPDVPYHWIRKQYTQSKDDAEERDHICQSE
TLEAHLKGMDELYK*

Genetic sequence of mEGFP

MKHHHHHHVSKGEELFTGVVPILVELDGDVNGHKFSVSGEGEGDATYGKLTLKFICT
TGKLPVPWPTLVTTLTYGVQCFSRYPDHMKQHDFFKSAMPEGYVQERTIFFKDDGNY
KTRAEVKFEGDTLVNRIELKGIDFKEDGNILGHKLEYNYNSHNVYIMADKQKNGIKV
NFKIRHNIEDGSVQLADHYQQNTPIGDGPVLLPDNHYLSTQSKLSKDPNEKRDHMVL
LEFVTAAGITLGMDELYK*

Additional Data

Bulk data fitting

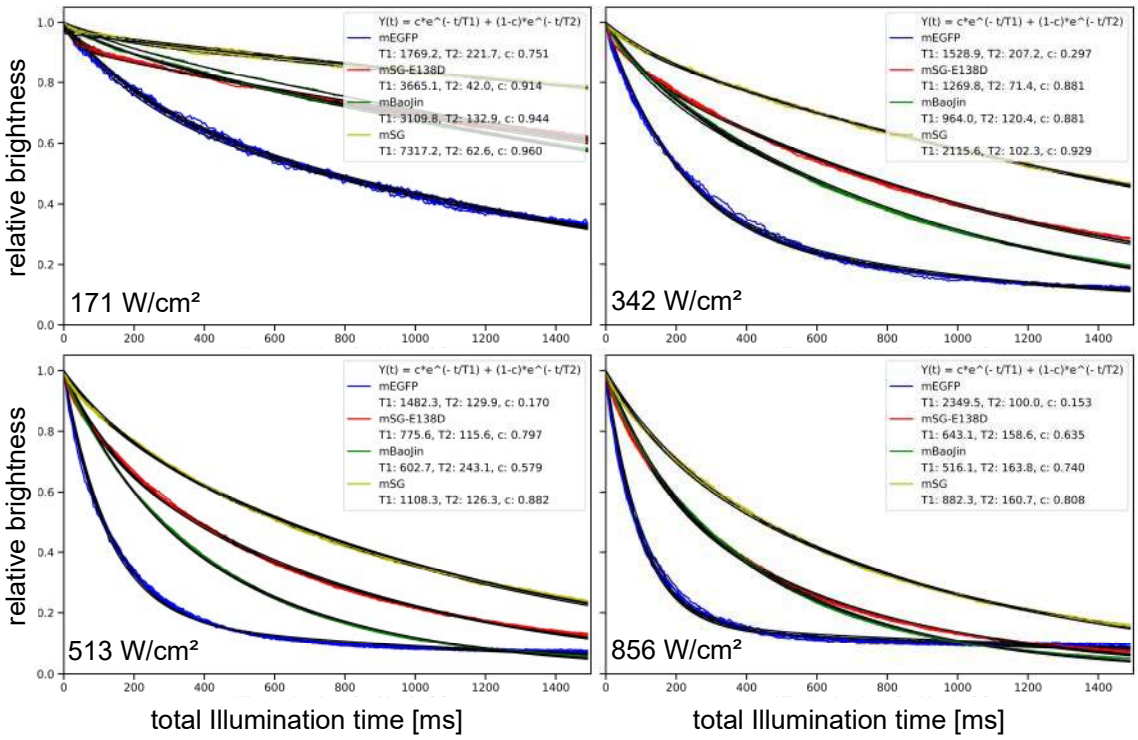

FIGURE A.1: The bulk bleaching curve measurements from Figure 3.1b, including the bi-exponential decay fitting displayed as black curves and the resulting c, T1 and T2 values in the graph for all four laser intensities measured, all four proteins used and five measurements per setting.

The following data represents the data from the single-molecule experiments performed on immobile lipid bilayers and were repeated three times (E1-E3). The number of recordings was adjusted to the actual protein surface density and resulted in E1 having 10 recordings per setting and protein (160 total), E2 including 15 recordings per setting and protein (240 total) and E3 including 5 recordings per setting and protein (80 total).

DaoSTORM + Python

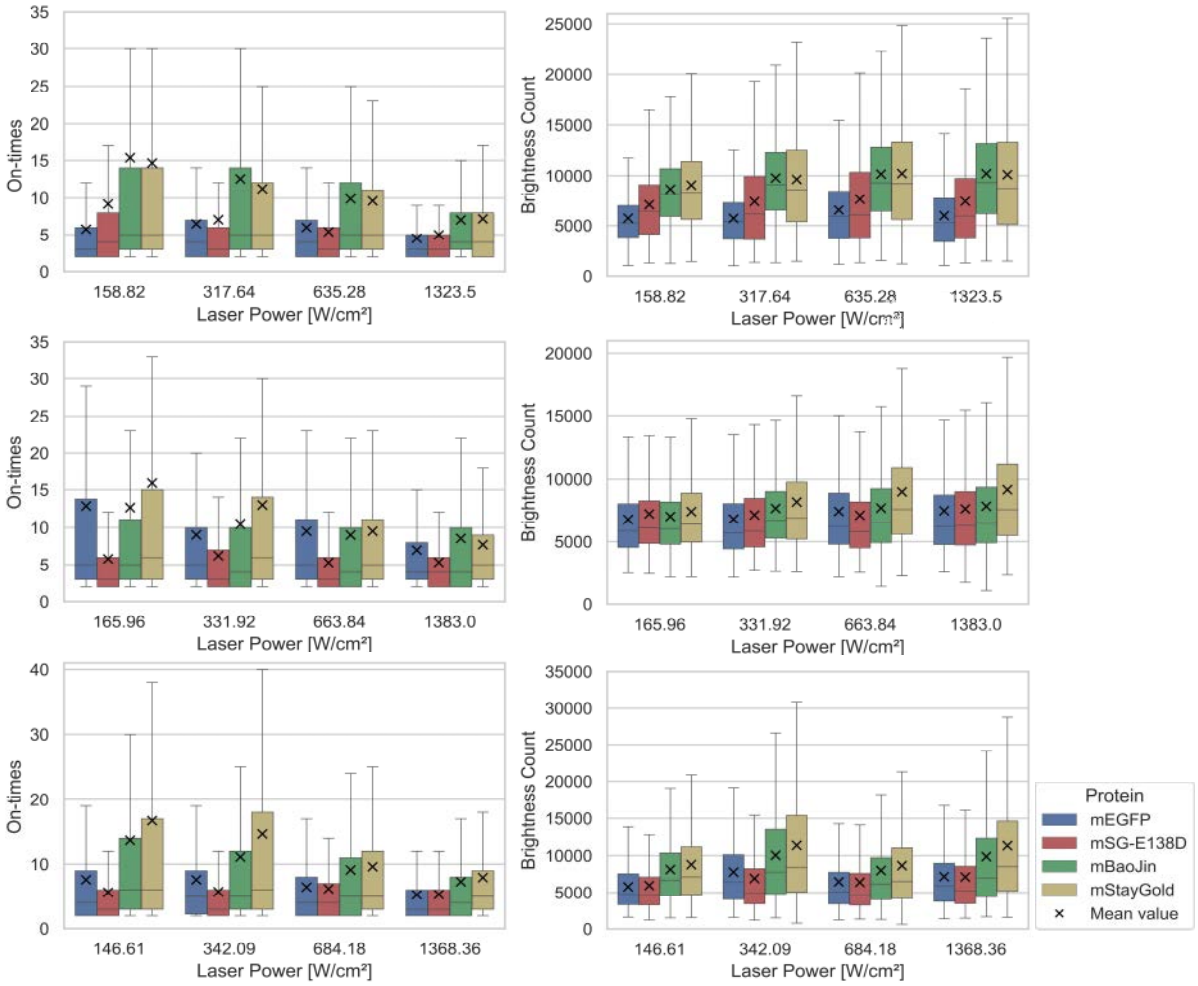

FIGURE A.2: The single-molecule on-time (left) and raw data brightness counts (right) distribution box plots and the mean values for E1-E3 localized using the *DaoSTORM* algorithm and the Python tracking are shown. The data from E1 (top) included 44794 particles, E2 (center) included 31509 particles and E3 (bottom) included 15458 particles.

ThunderSTORM + MATLAB

On-times

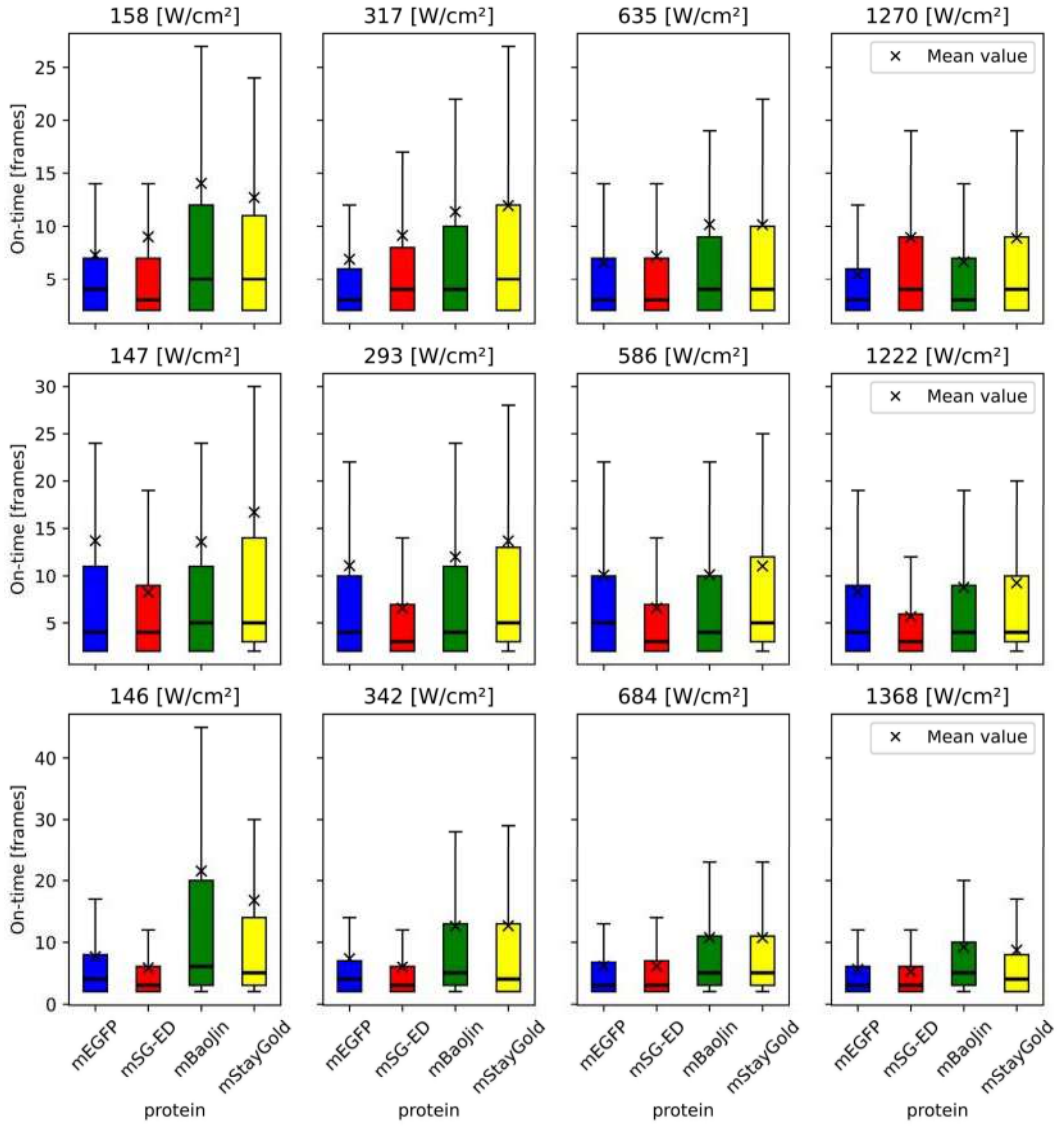

FIGURE A.3: The single-molecule on-times distribution box plots and the mean values for E1-E3 using the *ThunderSTORM* + MATLAB approach are shown for all four proteins and four laser intensities used. The data from E1 (top) included 262994 on-times, E2 (center) included 66624 on-times and E3 included 35792 on-times.

Off-times

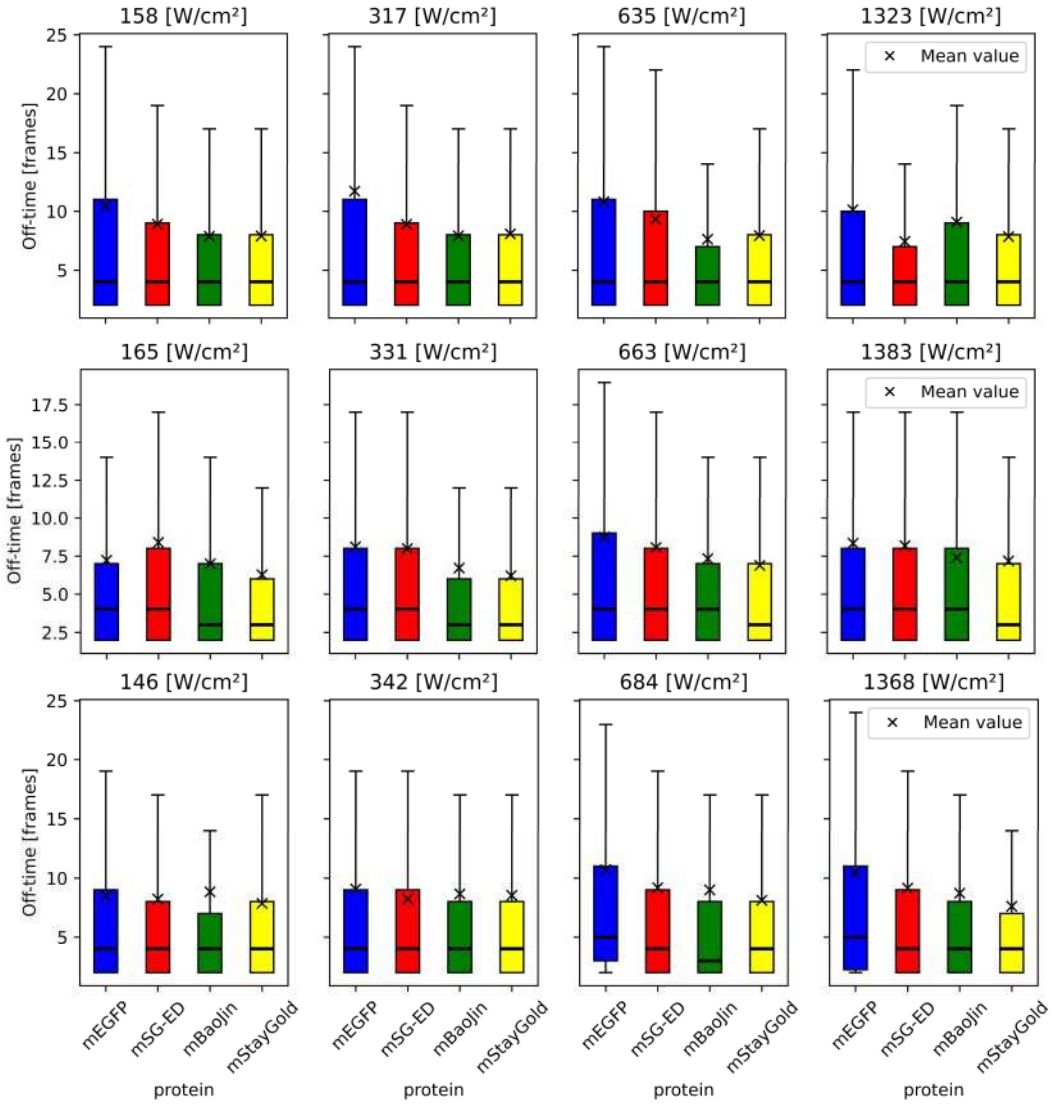

FIGURE A.4: The single-molecule off-times distribution box plots and the mean values for E1-E3 using the *ThunderSTORM* + MATLAB approach are shown for all four proteins and four laser intensities used. The data from E1 (top) included 237287 off-times, E2 (center) included 52890 off-times and E3 included 33858 off-times.

Number of localizations

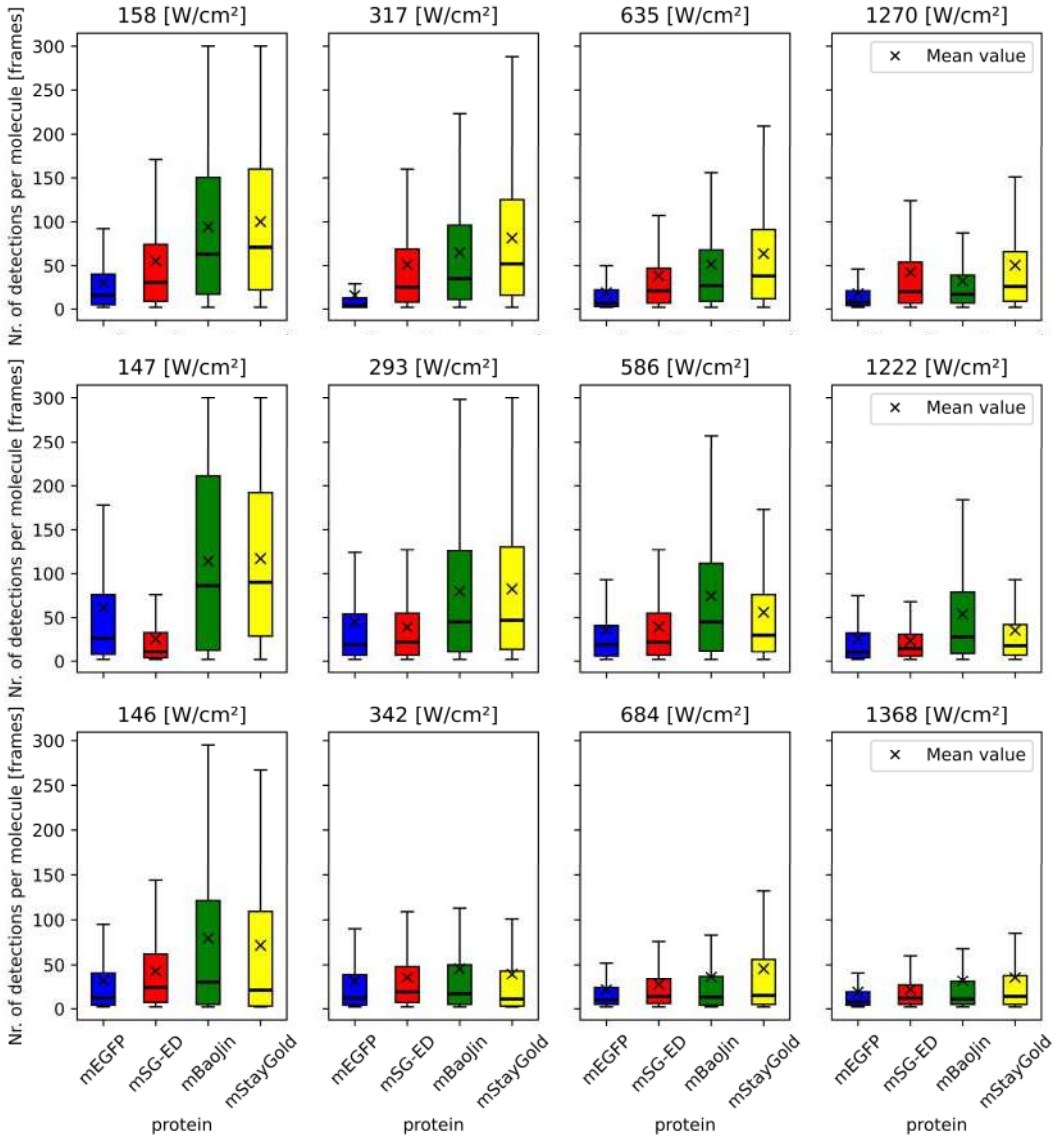

FIGURE A.5: The single-molecule number of localizations distribution box plots and the mean values for E1-E3 using the *ThunderSTORM* + MATLAB approach are shown for all four proteins and four laser intensities used. The data from E1 (top) included 57897 localitations, E2 (center) included 12856 localizations and E3 included 9302 localizations.

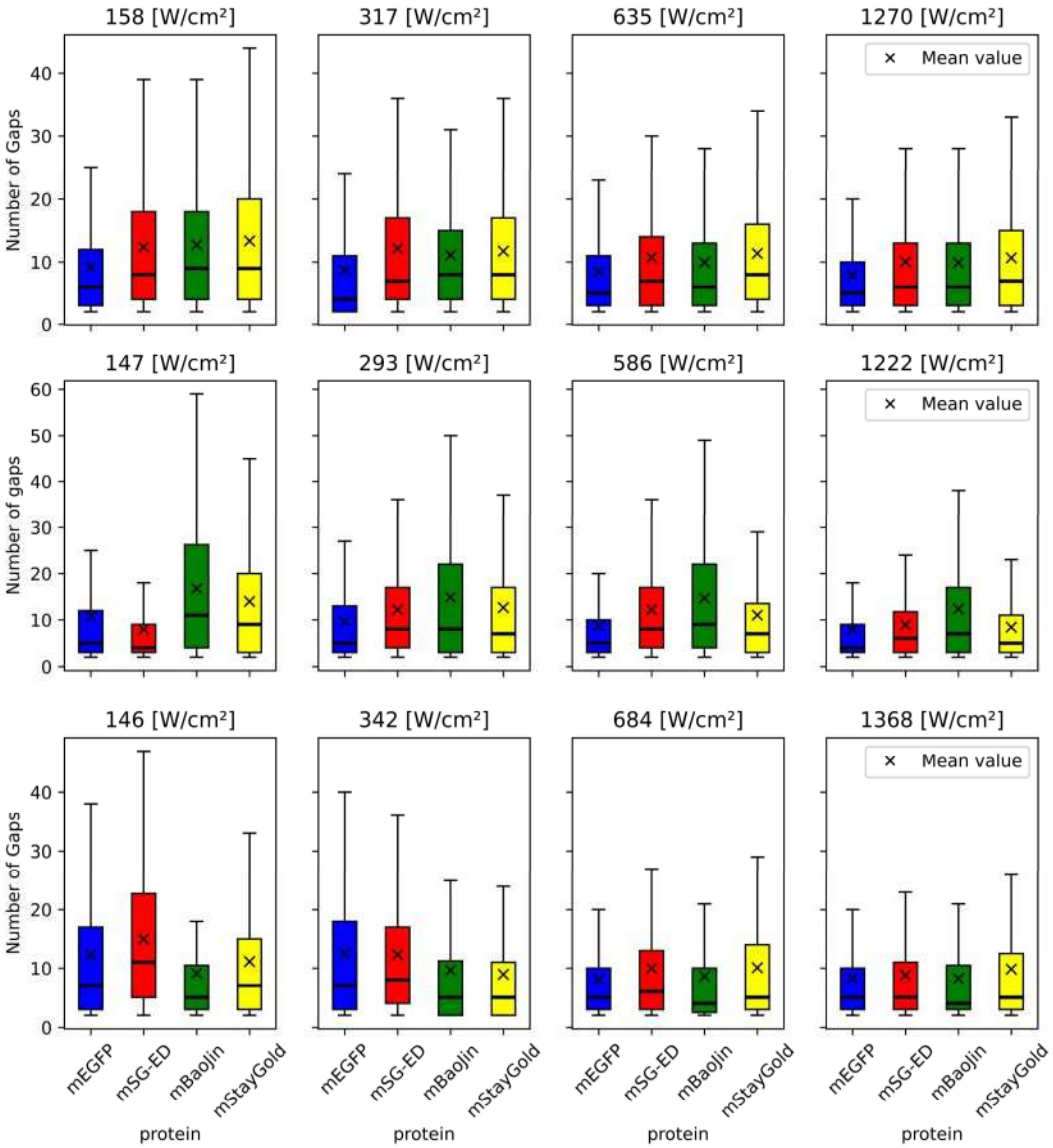

FIGURE A.6: The single-molecule number of gaps distribution box plots and the mean values for E1-E3 using the *ThunderSTORM* + MATLAB approach are shown for all four proteins and four laser intensities used. The data from E1 (top) included 37076 gaps, E2 (center) included 7726 gaps and E3 included 5133 gaps.

Measured half-time values

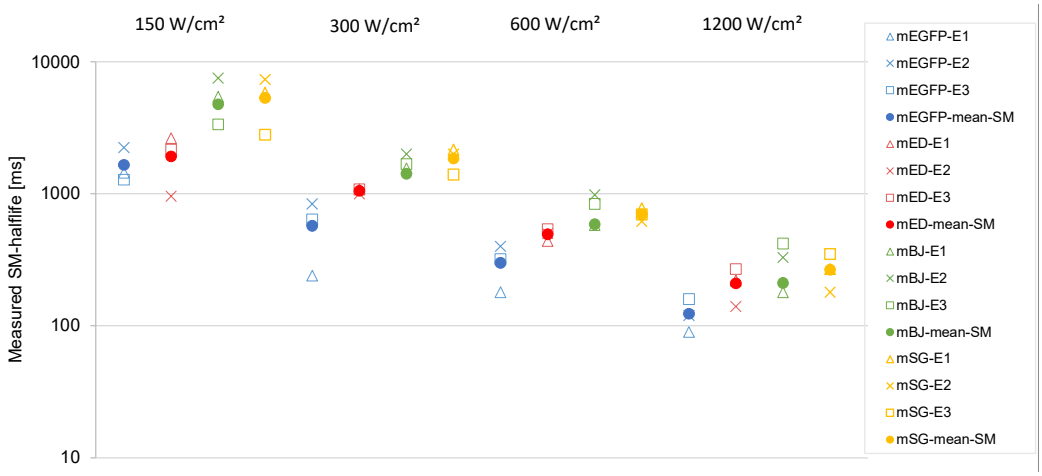

FIGURE A.7: Measured single-molecule half-lifes analyzing the single-molecule decay curves in the respective laser intensity settings per protein as a reference to the weighted calculated half-lifes.

Excitation dose dependence

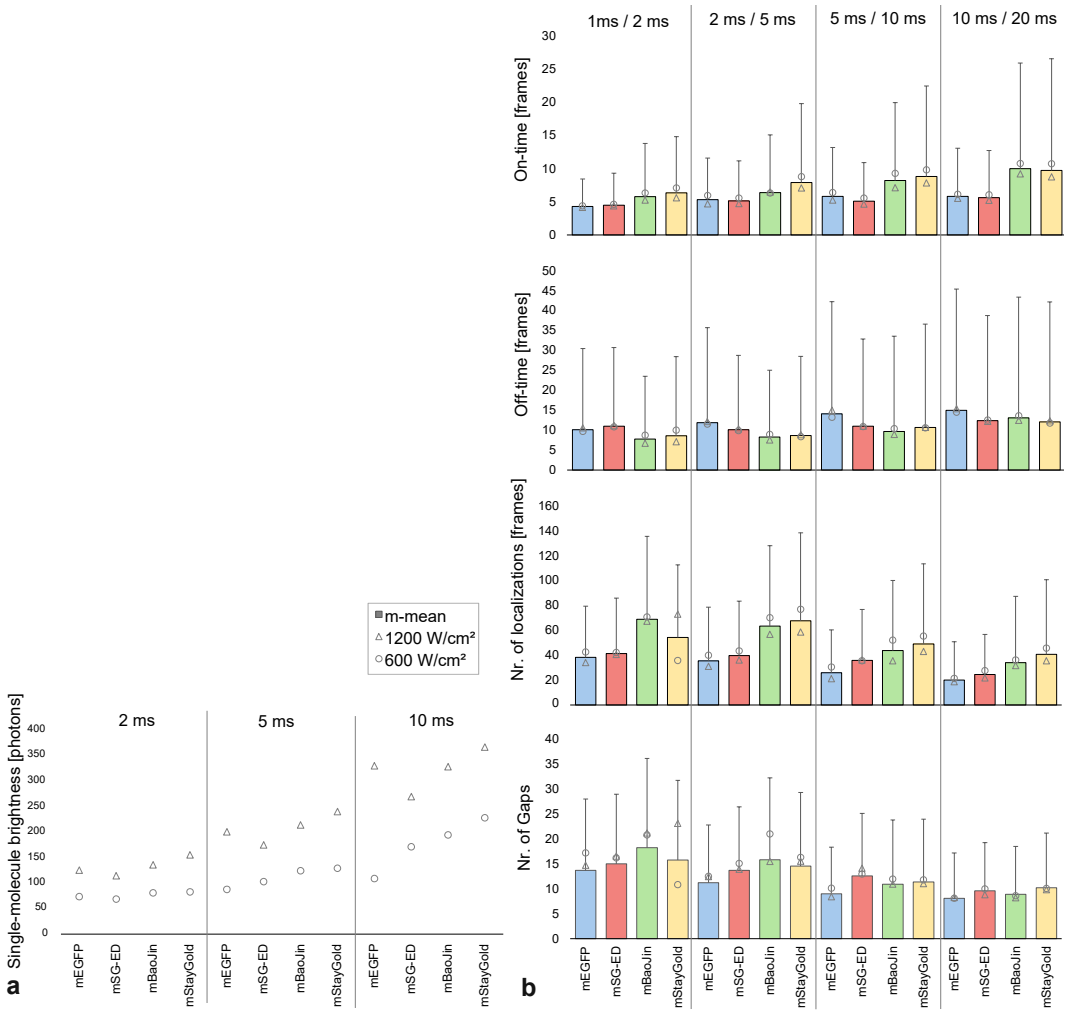

FIGURE A.8: The esulting mean values of: **a**, the single-molecule brightness, comaring the two laser intensity settings (600 W/cm² and 1200 W/cm²) at equal illumination times for all four fluorescent proteins; **b**, the blinking parameters for both excitation dose dependence experiments, including all four illumination time reduction steps. The first experiment using 1200 W/cm² laser intensity was performed at 10 ms, 5 ms, 2 ms and 1 ms illumination time (triangle) and the second experiment at 600 W/cm² laser intensity at 20 ms, 10 ms, 5 ms and 2 ms (square). The bars and the standard deviation represent all values measured at that specific setting.

Stroboscopic illumination data

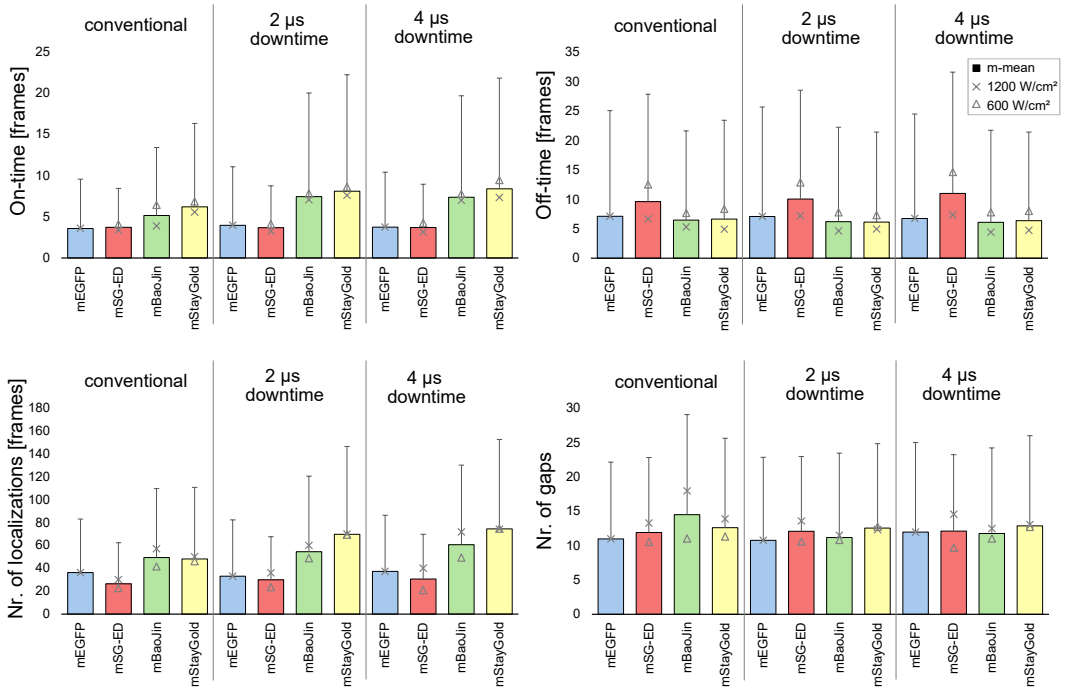

FIGURE A.9: Total single-molecule blinking results for conventional and stroboscopic illumination. The total illumination time was kept constant at 5 ms, while with stroboscopic illumination, 2500 pulses of 2 µs were used for one recording. The time between pulses (downtime) was varied between 2 or 4 µs. Depicted are the two individual experiments with laser intensities of either 600 W/cm² (triangle) or 1200 W/cm² (cross) and the solid bars represent the mean value and the standard deviation of the combined data.